

AFML-TR-72-133

Part IV

FG. (2)

AD A 024759

# THE RELATIONSHIPS OF STRUCTURE TO PROPERTIES IN GRAPHITE FIBERS

*RENSSELAER POLYTECHNIC INSTITUTE  
MATERIALS ENGINEERING DEPARTMENT  
TROY, NEW YORK 12181*

NOVEMBER 1975

TECHNICAL REPORT AFML-TR-72-133

Part IV

Approved for public release; distribution unlimited

AIR FORCE MATERIALS LABORATORY  
AIR FORCE WRIGHT AERONAUTICAL LABORATORIES  
Air Force Systems Command  
Wright-Patterson Air Force Base, Ohio 45433

9 DDC  
REFILED  
MAY 26 1976  
B

# NOTICE

When Government drawings, specifications, or other data are used for any purpose other than in connection with a definitely related Government procurement operation, the United States Government thereby incurs no responsibility nor any obligation whatsoever; and the fact that the Government may have formulated, furnished, or in any way supplied the said drawings, specification, or other data, is not to be regarded by implication or otherwise as in any manner licensing the holder or any other person or corporation, or conveying any rights or permission to manufacture, use, or sell any patented invention that may in any way be related thereto.

Copies of this report should not be returned unless return is required by security considerations, contractual obligations, or notice on a specific document.

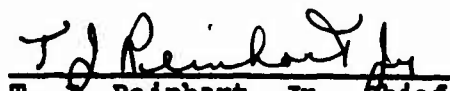
Part IV of this report was prepared by R. J. Diefendorf, Dennis M. Riggs and Ian W. Sorensen, Materials Division, Rensselaer Polytechnic Institute, Project 7342, "Fundamental Research on Macromolecular Materials and Lubrication Phenomena", Task 734202, "Studies on Structure-Property Relationships of Polymeric Materials" under contract AF33(615)-72-C-1422 entitled "The Relationship of Structure to Properties in Graphite Fibers". It was administered by the Air Force Materials Laboratory, Air Force Systems Command, Wright-Patterson Air Force Base. Mr. J. H. Ross, AFML/MBC, was the laboratory project monitor.

Part I of this report covered work conducted from 1 May 1970 to 31 April 1971. Part II covered work conducted from 1 May 1971 to 31 April 1972. Part III covered work conducted from 1 May 1972 to 31 April 1973. Part IV, the last report covered work conducted from 1 May 1973 to 31 April 1974.

The authors gratefully acknowledge the assistance of the Air Force, and in particular Mr. Jack Ross and the late Mr. Herbert M. Ezekiel who, as project monitors, supplied samples for testing. The authors deeply regret the untimely passing of Mr. Ezekiel.

  
J. H. ROSS  
Project Monitor

FOR THE COMMANDER

  
T. J. Reinhart, Jr., Chief  
Composites & Fibrous Materials Branch  
Nonmetallic Materials Division

AIR FORCE - 10 MAY 76 - 200

ACCESSION FOR	
NTIS	White Section <input checked="" type="checkbox"/>
DDC	Buff Section <input type="checkbox"/>
UNANNOUNCED	<input type="checkbox"/>
JUSTIFICATION .....	
BY .....	
DISTRIBUTION/AVAILABILITY CODES	
Dist.	Avail. and or SPECIAL
A	

UNCLASSIFIED

SECURITY CLASSIFICATION OF THIS PAGE (When Data Entered)

19 REPORT DOCUMENTATION PAGE		READ INSTRUCTIONS BEFORE COMPLETING FORM
1. REPORT NUMBER AFML-TR-72-133-Part 4	2. GOVT ACCESSION NO.	3. RECIPIENT'S CATALOG NUMBER
4. TITLE (and Subtitle) THE RELATIONSHIPS OF STRUCTURE TO PROPERTIES IN GRAPHITE FIBERS	5. DATE OF REPORT & PERIOD COVERED 1 May 73-31 Apr 74	
6. AUTHOR Russell J. Diefendorf, Dennis M. Riggs and Ian W. Sorensen	7. CONTRACT OR GRANT NUMBER(s) F33615-72-C-1422	
8. PERFORMING ORGANIZATION NAME AND ADDRESS Rensselaer Polytechnic Institute Materials Engineering Department Troy, New York 12181	10. PROGRAM ELEMENT, PROJECT, TASK AREA & WORK UNIT NUMBERS Nov 75 / 12 74	
11. CONTROLLING OFFICE NAME AND ADDRESS Air Force Materials Laboratory Air Force Systems Command Wright-Patterson Air Force Base, Ohio	12. REPORT DATE	
14. MONITORING AGENCY NAME & ADDRESS (if different from Controlling Office) HF-7342	13. NUMBER OF PAGES 66	
15. SECURITY CLASS. (of this report) Unclassified		15a. DECLASSIFICATION DOWNGRADING SCHEDULE
16. DISTRIBUTION STATEMENT (of this Report) Approved for public release; distribution unlimited. 734202		
17. DISTRIBUTION STATEMENT (of the abstract entered in Block 20, if different from Report)		
18. SUPPLEMENTARY NOTES		
19. KEY WORDS (Continue on reverse side if necessary and identify by block number) Composites Fibers		
20. ABSTRACT (Continue on reverse side if necessary and identify by block number) The anomalous density dip in PAN precursor carbon fibers has been investigated with respect to properties of commercial fibers and a series of specially heat-treated fibers. The density minimum is apparently due to a combination of two factors: the initial decrease in density caused by weight loss, and the subsequent density increase due to dimensional changes.		

UNCLASSIFIED

SECURITY CLASSIFICATION OF THIS PAGE (When Data Entered)

UNCLASSIFIED

SECURITY CLASSIFICATION OF THIS PAGE(When Data Entered)

Modes of failure in Fiber B and Kevlar I, III and IV fibers have been studied. The buckling of these fibers in compression is manifested as oblique strain markings. The strain band directions are used to show that Kevlar I is most ordered and Fiber B, the least.

The effect of abrasion on fiber strength has been studied qualitatively; abrasion does not appear to cause drastic reductions in strength.

CCA-1 rayon precursor carbon fiber and its replacements have been studied using optical microscopy and differential thermal analysis. The differences amongst the carbon fiber cloths and their precursors are substantial and can be expected to result in performance changes when CCA-1 is replaced by either substitute.

The microstructure of pitch-based carbon fibers has been studied using ordinary and polarized light microscopy. Variations in fiber shape and optical activity are related to the presence of both isotropic and mosophitic portions in the precursor pitch.

UNCLASSIFIED

SECURITY CLASSIFICATION OF THIS PAGE(When Data Entered)

# TABLE OF CONTENTS

Section	Page
I INTRODUCTION	1
A. Density Anomalies in PAN Precursor Carbon Fibers	4
B. High Modulus Organic Fiber Failure	5
C. Effects of Abrasion	5
II DENSITY ANOMALIES IN PAN PRECURSOR FIBERS	7
A. Heat-Treated AS Fibers	13
1. Experimental	13
2. Results and Discussion	16
B. The Nature of Carbon Fiber Porosity	22
C. Thermogravimetric Analysis	24
D. Homogeneity in Carbon Fiber Tows	31
E. Conclusions	34
III MODES OF FAILURE IN KEVLAR I, III, IV AND FIBER B	35
IV ABRASION AND FIBER STRENGTH	
A. Experimental	36
B. Results and Discussion	37
C. Conclusions	40
V COMPARISON OF CCA-1 RAYON PRECURSOR CARBON FIBER AND ITS REPLACEMENTS	41
A. Experimental	41
B. Observations and Discussion	42
C. Conclusions	55
VI MICROSTRUCTURE OF PITCH-BASED CARBON FIBERS	56
A. Experimental	56
B. Observations and Discussions	56
C. Conclusions	64

## LIST OF ILLUSTRATIONS

	Pag
1. Idealized schematic of crack propagation through highly oriented graphite.	3
2. The relation of density to modulus for the commercial carbon fibers AS, HTS, HMS, Morganite I and II and 5Y.	9
3. The relation of interplanar spacing ( $d_{0002}$ ) to modulus for commercial carbon fibers AS, HTS, HMS, Morganite I and 5Y.	10
4. Small angle X-ray scattering photographs for AS, HTS, HMS and Morganite I carbon fibers.	12
5. Schematic diagram of high temperature resistance heated graphite furnace.	14
6. Schematic diagram of heat-treated sample of fiber tow illustrating the use made of each part.	17
7. Percent length change versus heat-treatment temperature for heat-treated AS carbon fibers.	18
8. Density versus heat-treatment temperature for heat-treated AS carbon fibers.	20
9. Mean relative fiber diameters versus heat-treatment temperature for heat-treated AS carbon fibers.	21
10. Interplanar spacing ( $d_{0002}$ ) versus heat-treatment temperature for heat-treated AS carbon fibers.	23
11. Sample weight versus time for samples of HMS fiber tow immersed in various solvents (immersion time: 2 hours).	25
12. Sample weight versus time for samples of HMS fiber tow immersed in various solvents (immersion time: 48 hours).	26
13. Density versus heating rate of powdered samples of fully stabilized Courttelle fiber.	28
14. Final percent mass lost versus heating rate of powdered samples of fully stabilized Courttelle fiber.	29
15. Percent mass lost versus temperature for various heating rates of powdered samples of fully stabilized Courttelle fiber.	30

# LIST OF ILLUSTRATIONS (Continued)

	Page
16. Standard deviation of fiber bundle density versus carbon fiber modulus.	32
17. Histogram showing fiber bundle density distributions for AS, HTS, HMS and Morganite II carbon fibers.	33
18. Schematic diagram of tensile test fiber tow specimens.	38
19. Optical micrographs of rayon precursors mounted in epoxy.	43
a) "Old" ENKA rayon	
b) "New" ENKA rayon	44
c) IRC rayon	
20. Optical micrographs of carbon fibers from rayon precursors mounted in epoxy.	46
a) CCA-1	
b) CCA-2	47
c) CCA-2-1641-10	
21. Percent mass remaining versus thermocouple voltage and corresponding temperature for three rayon fibers.	48
22. DTA (difference in thermocouple voltage) versus thermocouple voltage and temperature for three rayon fibers.	50
23. Thermoanalyser trace for CCA-1 carbon fiber. (Heating rate: 8°C/min.)	51
24. Thermal analyser trace for CCA-2 carbon fiber. (Heating rate: 8°C/min.)	52
25. Thermal analyser trace for CCA-2-1641-10 carbon fiber. (Heating rate: 8°C/min.)	53
26. UCC pitch precursor carbon fibers (85msi): cross section.	54
a) Ordinary light	
b) Polarized light	
27. UCC pitch precursor carbon fibers (85msi): cross section.	58
a) Ordinary light	
b) Polarized light	
28. UCC pitch precursor carbon fibers (85msi): various angles of inclination.	60
a) Ordinary light	
b) Polarized light	

LIST OF ILLUSTRATIONS (Continued)

	Page
29. UCC pitch precursor carbon fibers (85msi): various angles of inclination.	61
a) Initially; polarized light	
b) After 45° counterclockwise rotation; polarized light	
30. UCC pitch precursor carbon fibers (20-30msi): cross-section.	62
a) Ordinary light	
b) Polarized light	
31. UCC pitch precursor carbon fibers (20-30msi): various angles of inclination.	63
a) Ordinary light	
b) Polarized light.	



## SECTION I

### INTRODUCTION

Over the past decade, the market for high performance fibers has expanded to the extent that a wide variety of fibers with greatly differing mechanical properties currently exists. However, carbon fibers, which form a significant portion of the total high performance fibers available, are limited in application by their low strain to failure, a problem that has remained unsolved. Newer low cost carbon fibers have shown even lower strains to failure. This report hopes to provide an understanding of the structure of some fibers and the relation between the structure and the physical properties of the fibers. Hopefully, the combination of this understanding with technology can provide major advances in the improvement of the mechanical properties of high performance fibers.

Although the theoretical strength of a material is determined by the modulus (simple calculations yield  $\sigma_{\text{theor}} \approx E/100$  to  $E/10$ ), other factors particularly the presence of flaws in brittle materials, limit the strength observed. In a typical brittle ceramic, such as non-graphitized carbon, the absence of plastic flow at the tip of a Griffith crack precludes the possibility of any stress relief by an increase in the radius of curvature at the crack tip. As a result, the stress concentration remains and the crack is free to propagate through the material under a relatively low applied stress. The strength-flaw relation in graphitic

materials is more complex, due to the relatively poor coupling between adjacent planes. In highly oriented graphite with easy shear, a propagating crack may be effectively stopped, as shown in Fig. 1, unless it extends through all the planes in the material. Hence, the microstructure and perfection of a graphite is important in determining its fracture behavior.

The flaw concentration in small samples of a material (such as fibers or whiskers) is much lower than in a larger body, hence the advantages of fibers in terms of strength. With a reduced concentration of flaws per unit length, it is possible, as in the case of whiskers, to attain near-theoretical strength. Fibers generally contain more flaws than whiskers but their availability in continuous form more than makes up for their lower strengths. The high strength per unit length of whiskers and fibers is of less value in a composite, if failure of one fiber causes failure of adjacent fibers and then the whole composite. Hence, not only are we interested in the flaw distributions in fibers for gauge lengths which approximate the part, but also at short gauge lengths which are equal to the overstressed region in a fiber adjacent to a broken fiber in a composite. The type of the flaws for these two differing gauge lengths is apt to be different, but the importance of determining the flaw sources to allow higher strength fibers to be made is obvious. This is especially true, since carbon fibers are limited in many applications by insufficient strain-to-failure. Thus, the importance of deter-

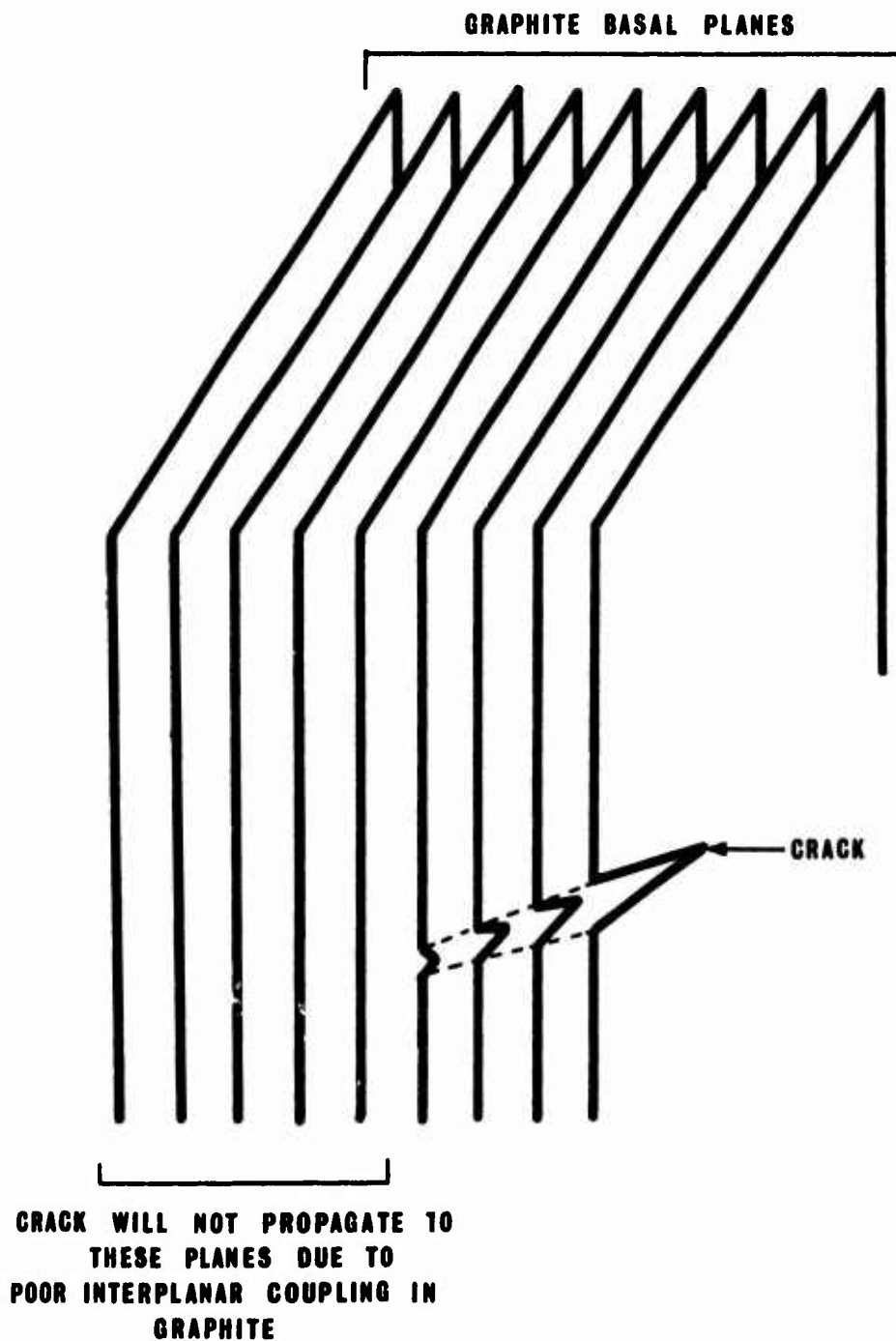


Fig. 1. Idealized schematic of crack propagation through highly oriented graphite.

mining the sources of these flaws is readily apparent.

In view of the importance of strength, considerable effort was expended on factors which might affect this property. The backgrounds for the three areas of strength studied, the "density dip" in PAN precursor carbon fibers, modes of failure in high modulus organic fibers and effects of abrasion, are outlined below.

A. Density Anomalies in PAN Precursor Carbon Fibers

Courtelle precursor carbon fibers first increase, then decrease in strength with increasing heat-treatment temperature while the modulus increases monotonically. These observations indicate drastic structural rearrangements taking place within the fibers. Both Courtelle and Orlon based carbon fibers show that the density versus heat-treatment passes through a minimum at a heat-treatment temperature where the strength decreases for Courtelle. It is also in this region that anomalies in  $d_{002}$  and  $L_c$  occur. If these phenomena could be more clearly understood in terms of the fiber structure, then it might be possible to apply this knowledge to the development of superior carbon fibers without the strength drop-off.

In the present work, an investigation of the density dip and related physical properties was made for a number of commercial fibers as well as a series of specially heat-treated AS fibers. Specifically, they were examined with regard to density, crystallography, preferred orientation, porosity, dimensional variations and optical microstructure.

## B. High Modulus Organic Fiber Failure

In the past, the microstructure of carbon fibers is assumed to be uniform along the length of the fiber. However, it has been noted that some carbon fibers show periodic variations along their length and the question arises as to whether or not these inhomogeneities are a source of flaws and hence, low strength. Some of these inhomogeneities arise during air stabilization of PAN precursor fibers and manifest themselves as optically visible "transverse strain bands". They are a result of the slow tensile strain rate accompanying the conversion of precursor material to a ladder polymer and are still visible in the final carbon fiber product.

We have applied the same technique to high modulus organic fibers. Similar but oblique, strain bands have been observed in the failure of Kevlar I, III, IV and Fiber B. These fibers have poor compressive properties in composite form but it was uncertain whether the fiber itself was the cause. In the present work, optical studies of strain bands have been made on polyaramides.

## C. Effects of Abrasion

Since surface flaws play such an important role in the strength and fracture characteristics of materials such as carbon, anything which tends to introduce surface flaws into the material must be carefully controlled. Although high performance fibers may have fairly low surface flaw concentrations immediately following their formation, every succeeding step in processing, packaging, shipping,

etc. before the final layup in a composite may introduce flaws through abrasion. Although studies have been made to show the effect of abrasion on relatively flaw free specimens, no work has been done on a fiber such as AS to see the effect of further abrasion on the already fully processed fiber in the as-received condition. Thus, it should be possible to determine whether abrasion introduced after manufacture but prior to composite fabrication exerts an important influence on the strength or if the worst flaw introduction occurs during the manufacturing process itself. This would indicate whether or not careful handling techniques should be utilized at the user level to achieve maximum average fiber (and composite) strength as well as minimizing the scatter of individual fiber strengths.

In addition to the studies of strength, two other separate areas were investigated in the present work. A comparison of low modulus carbon fibers CCA-1, and two varieties of CCA-2 in addition to a study of their rayon precursors was made to determine if significant differences may exist amongst them. CCA-1 carbon fiber cloth has been used in high temperature applications such as nozzle inserts and heat shields for rockets. However, the precursor for this fiber made by Industrial Rayon Corporation is no longer available and the substitutes "ENKA" and "new ENKA" have been tried as replacements. In the present work, an attempt is made to compare the old and new fibers with respect to microstructure and thermal analysis

so that areas of significant difference will be pinpointed without resorting to exhaustive qualification testing.

A major limitation of many present-day carbon fibers is high cost. Fiber processes based on petroleum pitch which costs only a few cents a pound provide much potential for cost reduction. In view of this, work was initiated on the characterization of two such fibers supplied by Union Carbide.

## SECTION II

### DENSITY ANOMALIES IN PAN PRECURSOR FIBERS

The axial microstructures of PAN precursor fibers consist of undulating graphite ribbons 30 to 120Å thick, which are roughly parallel to the fiber axis. While the radial microstructures show variety, the fiber surfaces are generally found to have a strong preferred orientation of the graphite basal planes parallel to the surface. Upon heat-treatment, the amplitude of the ribbons decreases and the fiber modulus increases. If this straightening of ribbons is associated with a length increase, then the density might be observed to decrease, since the onion-skin radial microstructure would tend to maintain diameter. The net effect would be a decrease in carbon atoms per unit cross-section, and more probably the formation of microcracks. Both would lead to decreases in strength. The following work was performed to see if there was a correlation between density and strength.

The initial experiments were performed on the following commercial fibers made from Courtelle: AS, HTS, HMS (Hercules); MI, MII (Morganite); 5Y (Fortafil). Mean fiber bundle densities were obtained using a density gradient column composed of bromoform and carbon tetrachloride. Mean bundle density is plotted as a function of modulus in Fig. 2. The density increases as the Courtelle is carbonized, but with further heat-treatment, a minimum in density is observed at a modulus of about 38-40MSI.

Diffraction measurements of d-spacing as well as small angle X-ray scattering were utilized in an attempt to determine the factors causing the density dip anomaly. D-spacings for the 0002 planes were obtained on the diffractometer and are plotted as a function of fiber modulus in Fig. 3. The d-spacing is observed to increase with modulus up to a value of about 39 MSI. At higher modulus values, the d-spacing begins to drop off in a continuous fashion. However, although both LeMaistre and Tokarsky found density minima, the former found a constant  $d_{0002}$  on Courtelle precursor samples prepared at R.P.I. while the latter observed wide variations in  $d_{0002}$  in the commercial, Courtelle precursor fibers at the density minimum. While it might appear that the  $d_{0002}$  spacing could be an explanation for the drop in density, for the data shown, the density changes are much larger proportionally than the  $d_{0002}$  variation.

Since the d-spacing change is insufficient to explain the



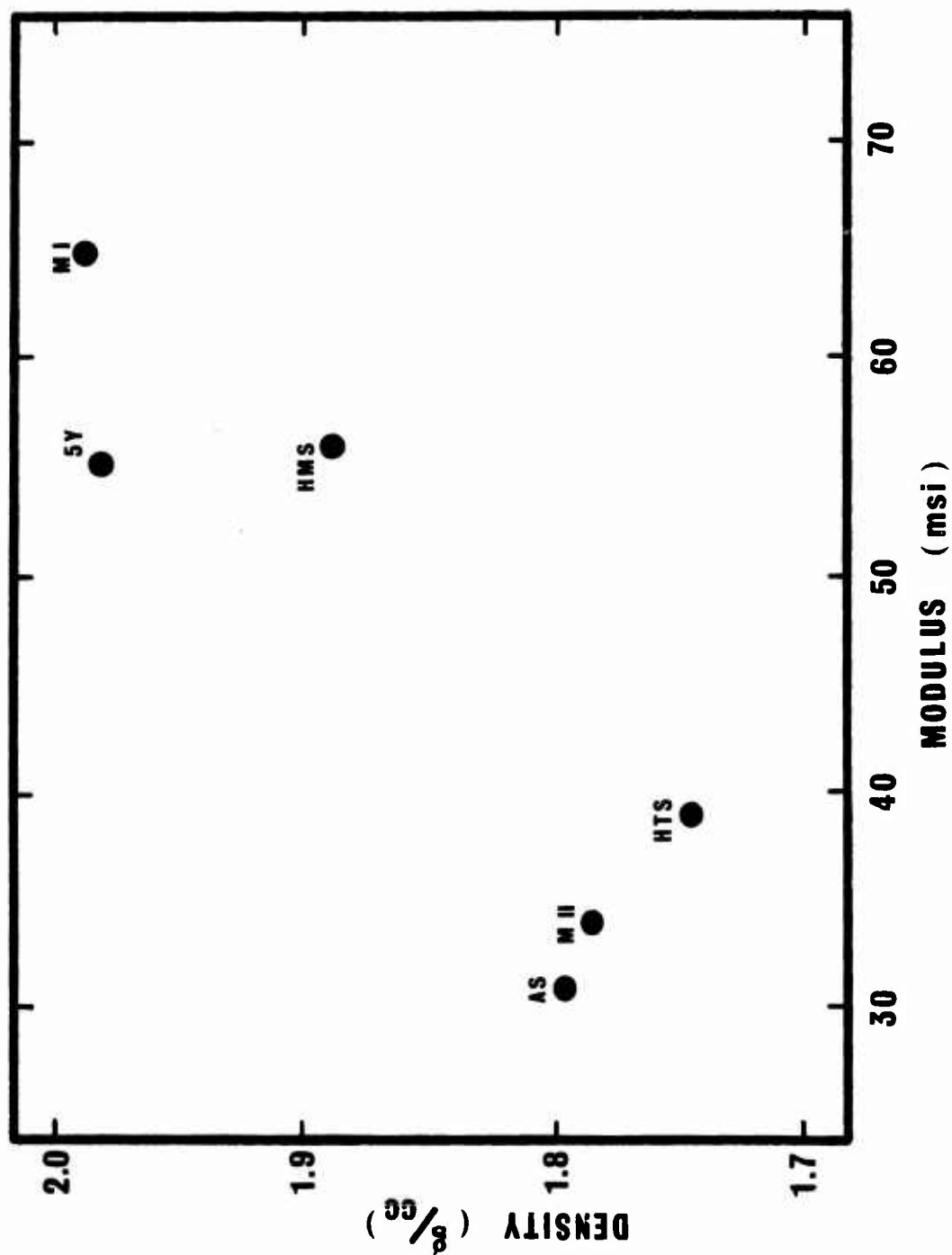


Fig. 2. The relation of density to modulus for the commercial carbon fibers AS, HTS, HMS, Morganite I and II and 5Y.

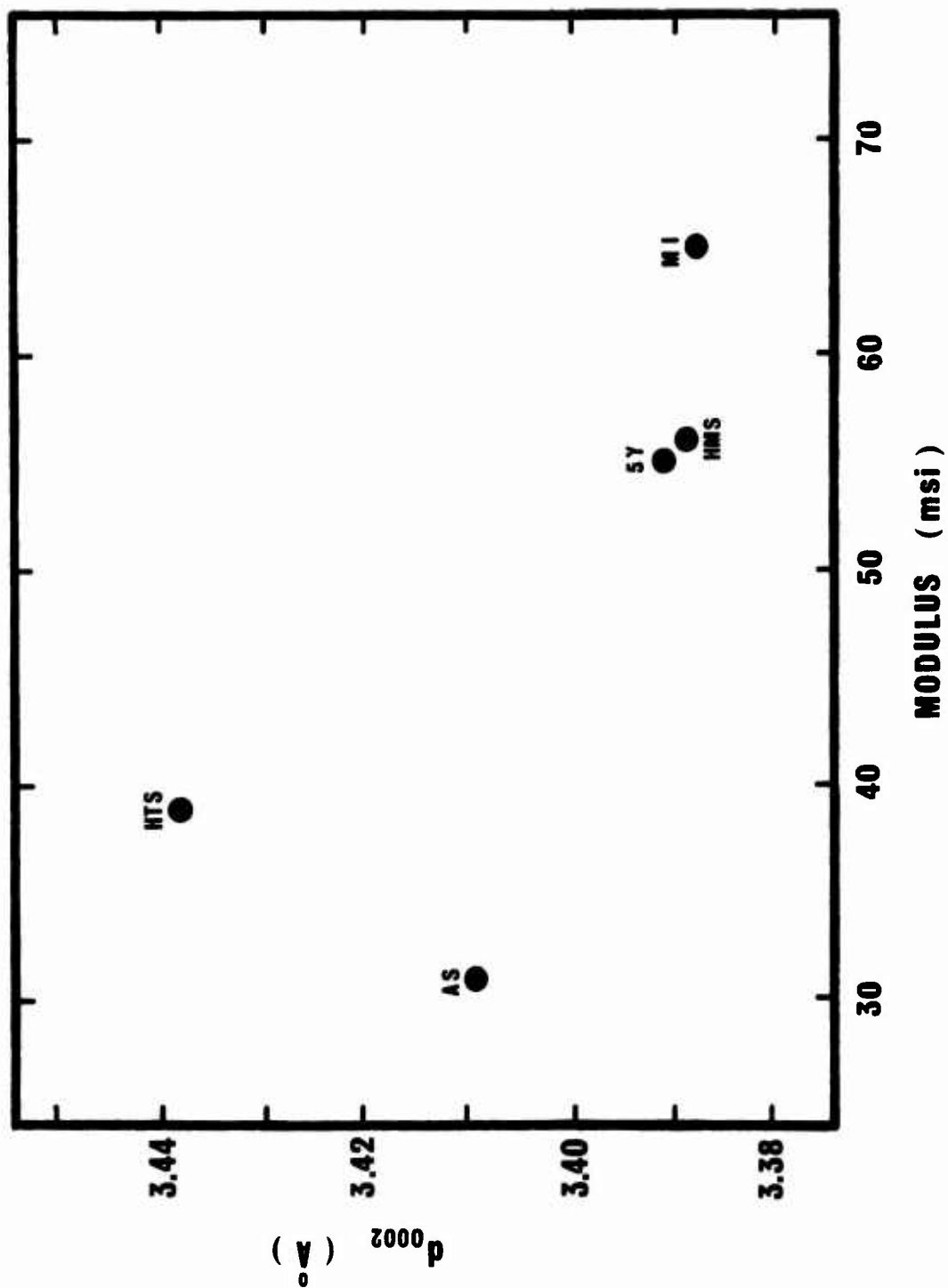


Fig. 3. The relation of interplanar spacing ( $d_{002}$ ) to modulus for commercial carbon fibers AS, HTS, HMS, Morganite I and 5Y.

density dip, a question now arises as to the cause of this porosity change. It has been shown that in the region of the density dip and hence the "porosity maxima", a significant degree of optical activity begins to develop in the fiber cross-sections. This increased optical activity corresponds to the development of the radial as well as axial structure in the fibers. Hence, it may be assumed that the degree of porosity changes to a maximum when the microfibrils in the relatively poorly structured AS fiber begin to straighten out upon further heat-treatment to a condition corresponding to HTS. With more heat-treatment, the axial and radial structures are known to develop to a high degree, but the corresponding dimensional changes are small. Tokarsky has shown that at high heat-treatment temperatures, circumferential compressive stresses develop which should be expected to squeeze out the porosity. This would be expected in the highly heat-treated HMS fiber which exhibits a high density.

Small angle X-ray scattering photographs for AS, HTS, HMS and MI, Fig. 4, tend to confirm this. Two qualitative observations may be made, namely: (1) there is an initial increase in fine porosity (indicated by increased small angle scattering) with increasing modulus and then a decrease which corresponds to the changes in density; (2) the porosity becomes more aligned to the fiber axis as the modulus increases. However, there is a large amount of very small angle scattering in all samples such that the change

**AS**  
**E = 31 msi**



**HTS**  
**E = 39 msi**



**HMS**  
**E = 56 msi**



**M I**  
**E = 65 msi**



**Fig. 4.** Small angle X-ray scattering photographs for AS, HTS, HMS and Morganite I carbon fibers.

in total porosity with increasing modulus cannot be determined.

#### A. Heat-Treated AS Fibers

Comparison of the properties such as density of commercial carbon fibers can be difficult - since each fiber is processed differently and the effects of processing variations may affect the resulting property comparisons. Also, it is not possible to determine such things as length changes during heat-treatment of such fibers. Thus, it was decided to heat-treat samples of a lower modulus fiber (in this case AS) to a variety of temperatures above its nominal heat-treatment temperature of about 1200°C. In this way, all parameters except for HTT can be considered fixed and so the scatter of measured relations should be reduced. Also, the number of samples can be made greater so that intervals between heat-treatment temperatures are smaller and a more precise curve can be drawn through the points.

1. Experimental. The AS fiber samples were heat-treated in a high temperature resistance heated graphite vacuum furnace (a schematic of which is shown in Fig. 5). This furnace permitted use of a rough vacuum (about .1 torr) or a gaseous atmosphere and provided constant temperature along its length.

For heat-treatments up to 2000°C, a rough vacuum was used; above 2000°C the runs were made under approximately one atmosphere of argon to prevent deterioration of the furnace and the fibers themselves due to the increased vapor pressure of the carbon at

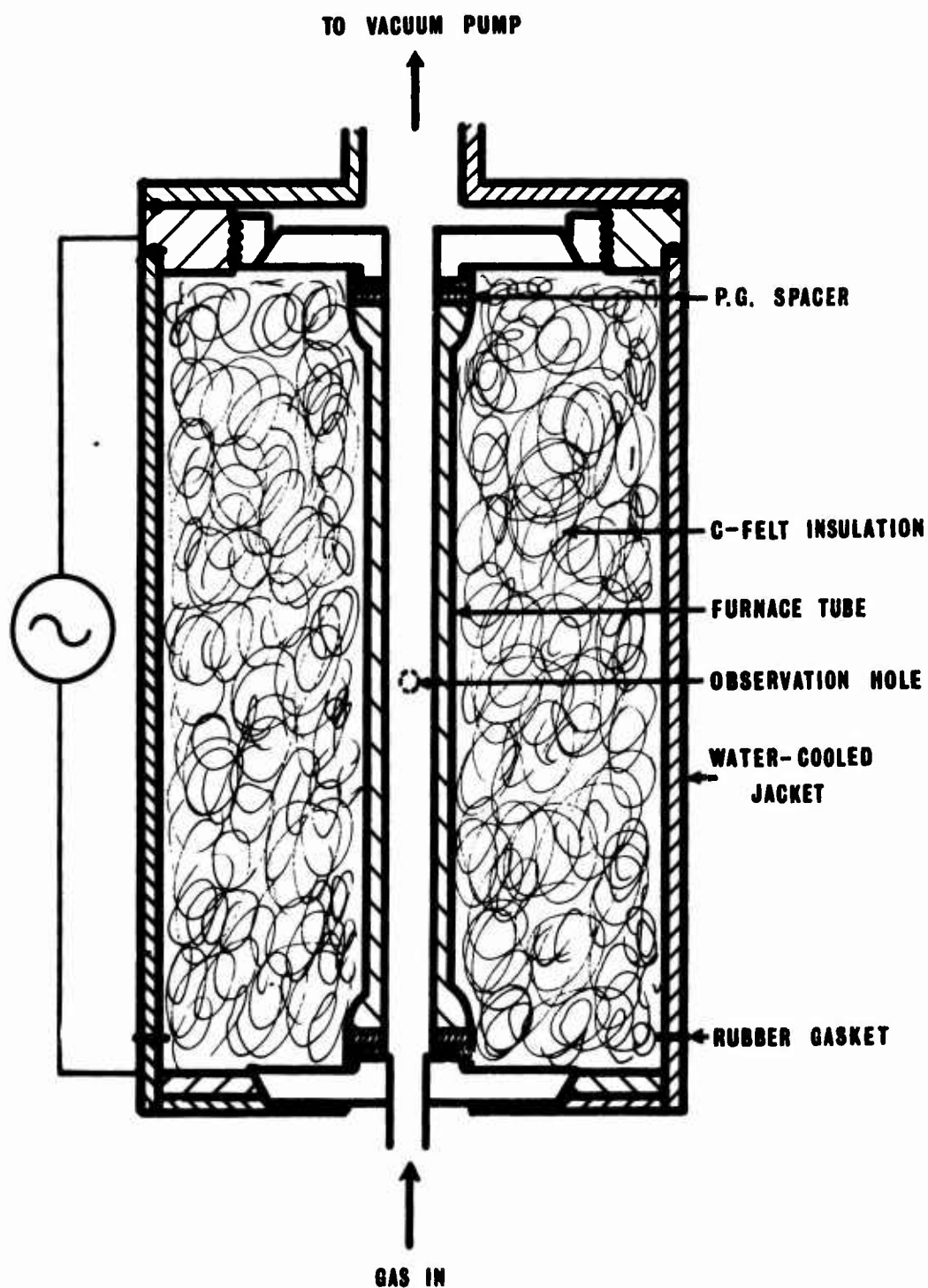


Fig. 5. Schematic diagram of high temperature resistance heated graphite furnace.

elevated temperatures.

Each AS specimen consisted of a length of tow approximately 20cm in length. To facilitate measurement of length changes in the heat-treated fibers, fiducial marks were made on each specimen by securing a loop of carbon fiber strand with a small drop of white glue near each end of the tow. Although the glue carbonized upon heating, enough residue remained to prevent the fiducial marks from accidentally moving when the specimens were inserted or removed from the furnace tube. Measurements of the distance between the marks on each specimen before and after each run were made and compared. No attempt was made to hold the run at temperature; once the desired point was reached, power was cut and the furnace began to cool-off immediately. Furnace cooling normally took from one-half hour to an hour depending on the final heat-treatment temperature. When cool, the system was repressurized and the sample removed for observation and physical testing.

The specimen length was remeasured and the density was determined in quadruplicate. One section of the remaining parts of the sample was mounted for observation and determination of average fiber diameter. Care was taken to ensure the perpendicularity of the specimen in the mold. Also, the end of the tow chosen for observation was that which had been near the longitudinal center of the furnace tube and for which the exact temperature of heat-treatment was most reliably known (the pyrometer only measured fiber temperatures

in the central section of the furnace tube). Figure 6 illustrates a sample tow and the use made of each part.

The mounted sample was ground and polished and then observed under an optical microscope at a magnification of 400X. The diameters of the individual fibers were measured by means of a filar eyepiece attachment. Fifty individual diameter measurements were made on each specimen to ensure some statistical significance. The fifty were taken in groups of ten to twelve from different areas of the cross-section, while the measurements in each group were made in a random way. The mean and standard deviation for the sample was then calculated. The mounted specimen was also observed under polarized light to detect changes in the optical activity attributable to changes in the fiber structure.

The fibers used in the density determination were mounted in a diffractometer for measurement of the  $d_{0002}$  planar spacing in the fibers. Corrected d-spacings were used to show the relative magnitudes and general trend of the d-spacings with increasing heat-treatment temperature.

2. Results and Discussion. The percent length change as a function of heat-treatment temperature is shown in Fig. 7. Despite considerable scatter, there is a definite positive slope to a best-fit line drawn through the points. The shrinkage in fibers heat-treated at lower temperatures refutes the theory that a length increase occurs upon heat-treatment when the wrinkled fibrils straighten.



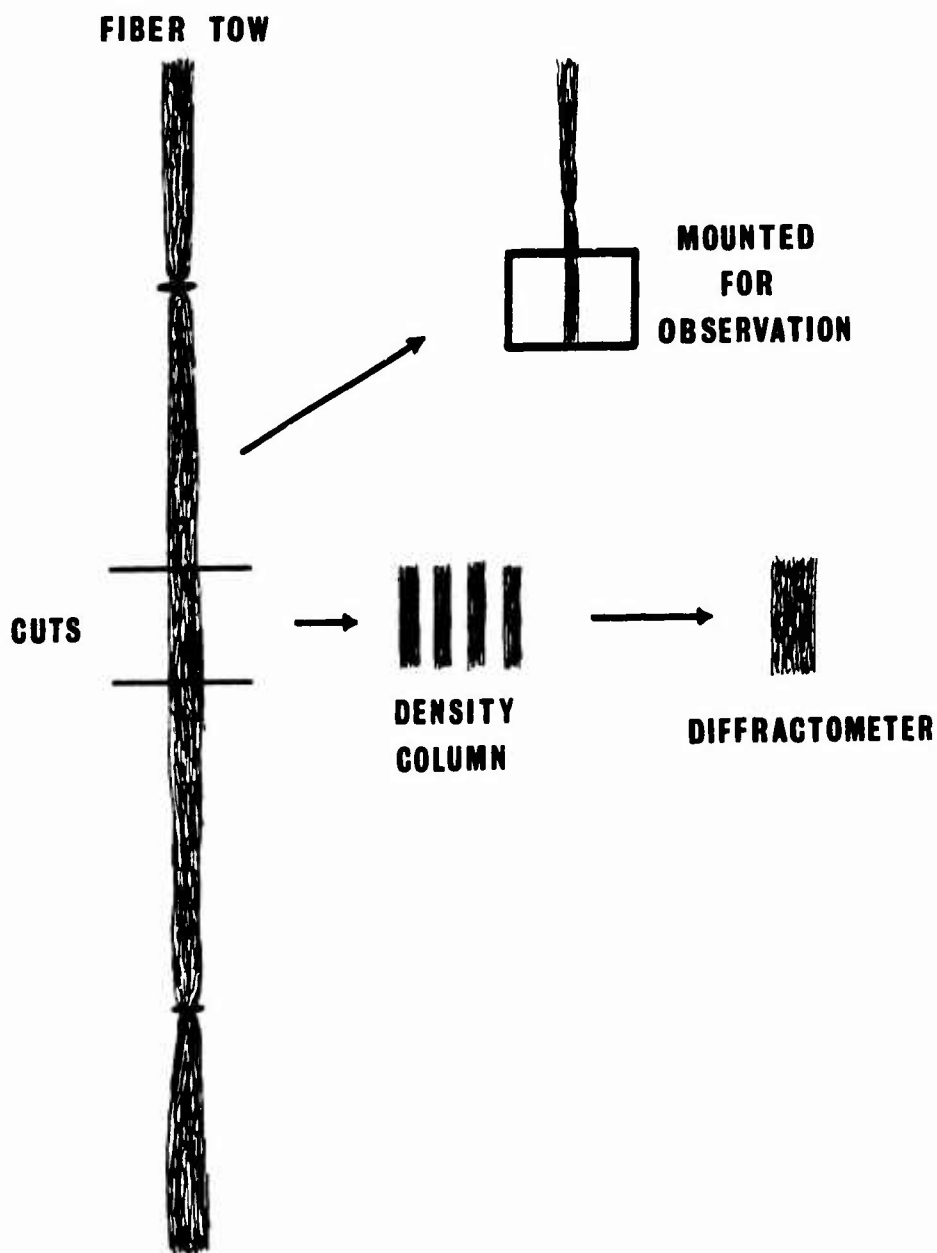


Fig. 6. Schematic diagram of heat-treated sample of fiber tow illustrating the use made of each part.

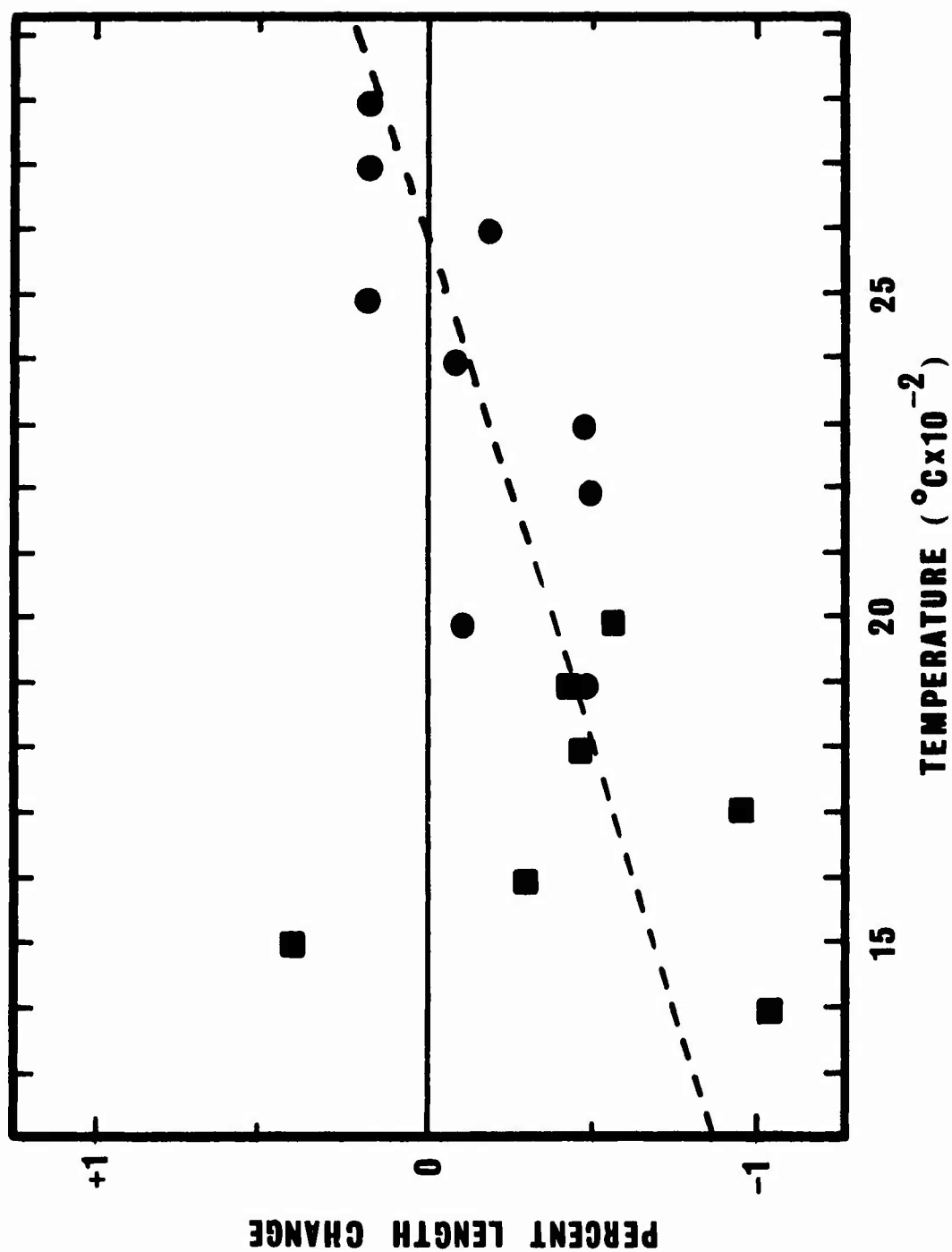


Fig. 7. Percent length change versus heat-treatment temperature for heat-treated AS carbon fibers.

The specimen density versus heat-treatment temperature is shown in Fig. 8. A fairly broad minimum is reached around 1900°C-2000°C above which the density increases with further heat-treatment. The density at 2800°C is well below the theoretical value of 2.264gm/cc, but only slightly less than the value of 2.087gm/cc, which is the value that would result from cooling a fully dense onion-skin cross-section fiber from 2800°C to room temperature. When compared with the density dip observed with the commercially processed fibers AS, HTS and HMS in Section II, the curve is seen to be much less pronounced. This could result from the shorter time at temperature encountered in the present work compared to the commercial processes. However, results obtained by LeMaistre in this laboratory using a similar high heating rate to final temperature had a very sharp density minimum, but the heating included carbonization.

The mean relative fiber diameters as a function of heat-treatment temperature are shown in Fig. 9; as well as the standard error. The sample size for each specimen was fifty but with the inherently broad band of diameter scatter for Courtelles precursor fibers, the subtle changes in diameter expected upon heat-treatment are difficult to determine. A least squares analysis of the data, assuming a linear relation, indicates a slight decrease in diameter with increasing heat-treatment temperature. Combining this trend with the length trend, and assuming no weight loss, the increase in density above the density minimum is predicted well. Hence,

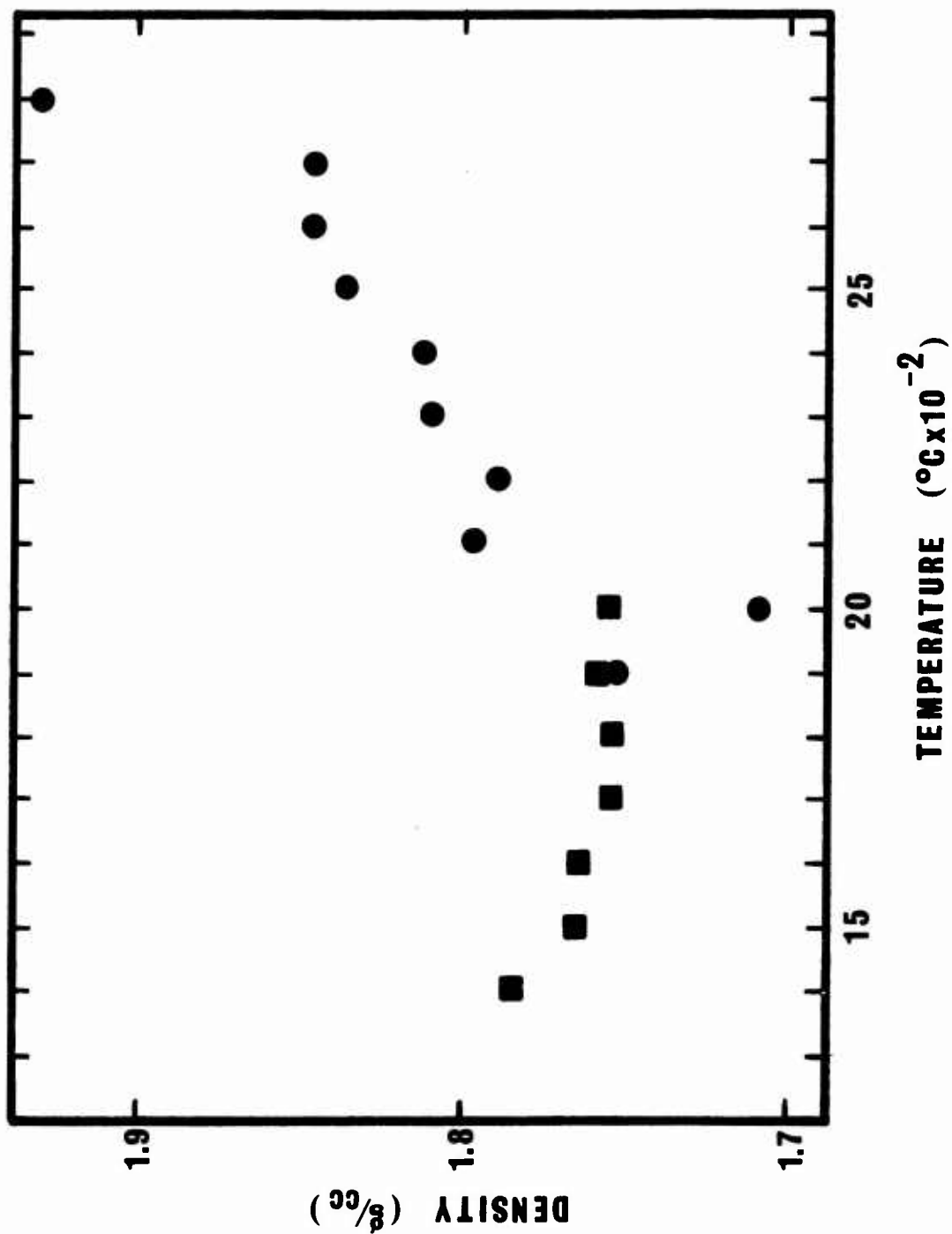


Fig. 8. Density versus heat-treatment temperature for heat-treated AS carbon fibers.

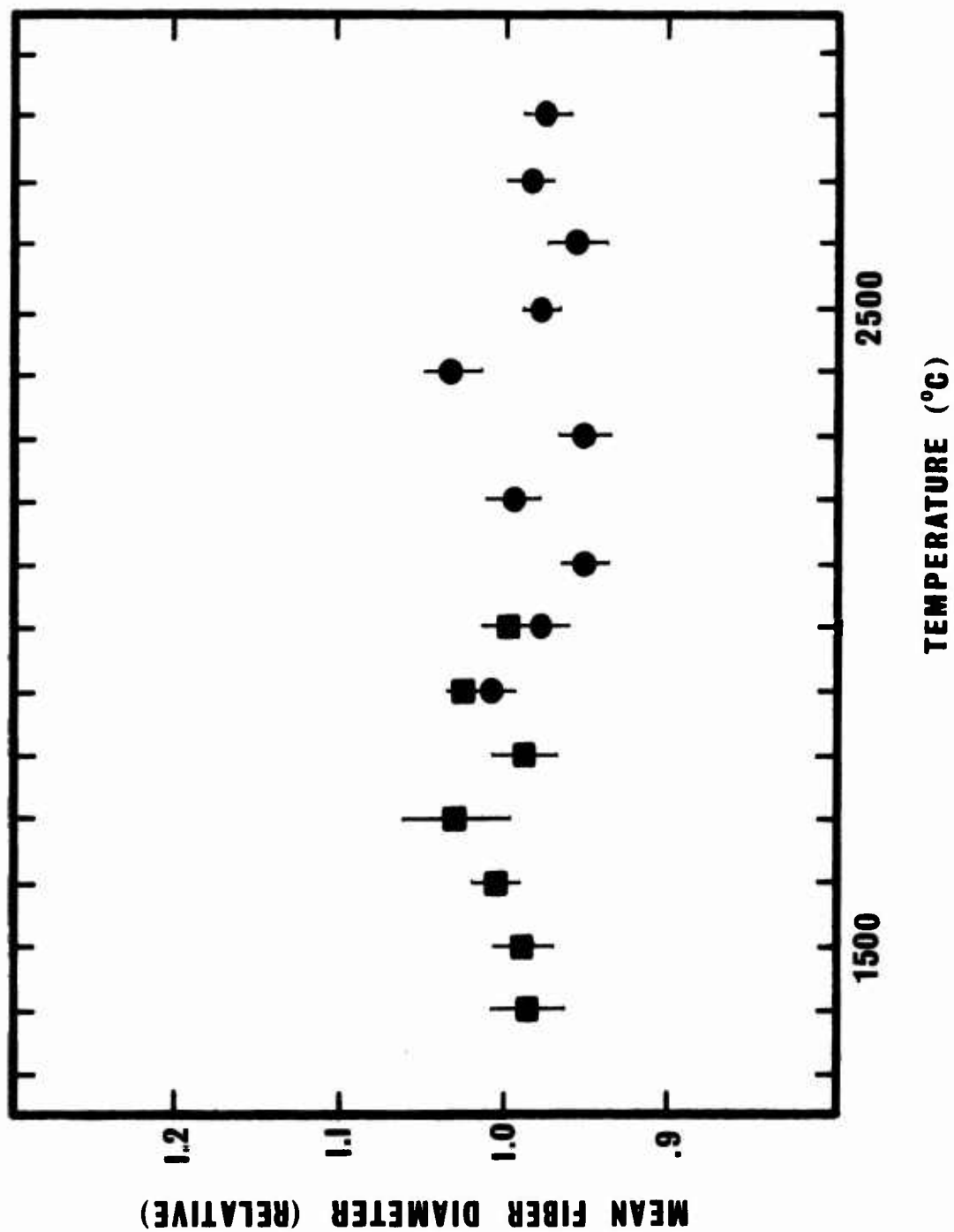


Fig. 9. Mean relative fiber diameters versus heat-treatment temperature for heat-treated AS carbon fibers.

the observed length and diameter trends are probably real. The fit below the density minimum is poor, and either the assumption of zero weight loss, or a change in porosity is probably responsible.

The corrected d-spacings obtained from the diffractometer are plotted versus heat-treatment temperature in Fig. 10. Clearly, the  $d_{0002}$  spacing decreases with heat-treatment, although considerable scatter exists. The source for the scatter in the heat-treating schedule is not known, but most likely is related to the short hold time at the maximum temperature.

#### B. The Nature of Carbon Fiber Porosity

If the density dip anomaly is a result of porosity caused by structural changes opening up voids, then it is advantageous to know what kind of porosity it is, i.e., open or closed. Using the density gradient column technique, open porosity, where the solvent is able to penetrate the pores will result in higher density estimates than closed porosity where the solvent cannot enter the voids. That solvents could enter fiber pores might be indicated by work at the Aerospace Corp. where, in a personal communication, they claimed higher strength and modulus for fibers immersed in acetone.

To determine if porosity might be affecting observed densities, samples of AS and HMS were immersed in a variety of solvents: acetone, benzene, carbon tetrachloride, bromoform, and water for time periods of up to 48 hours. The fibers (which had been initially weighed) were removed from the solvents and allowed

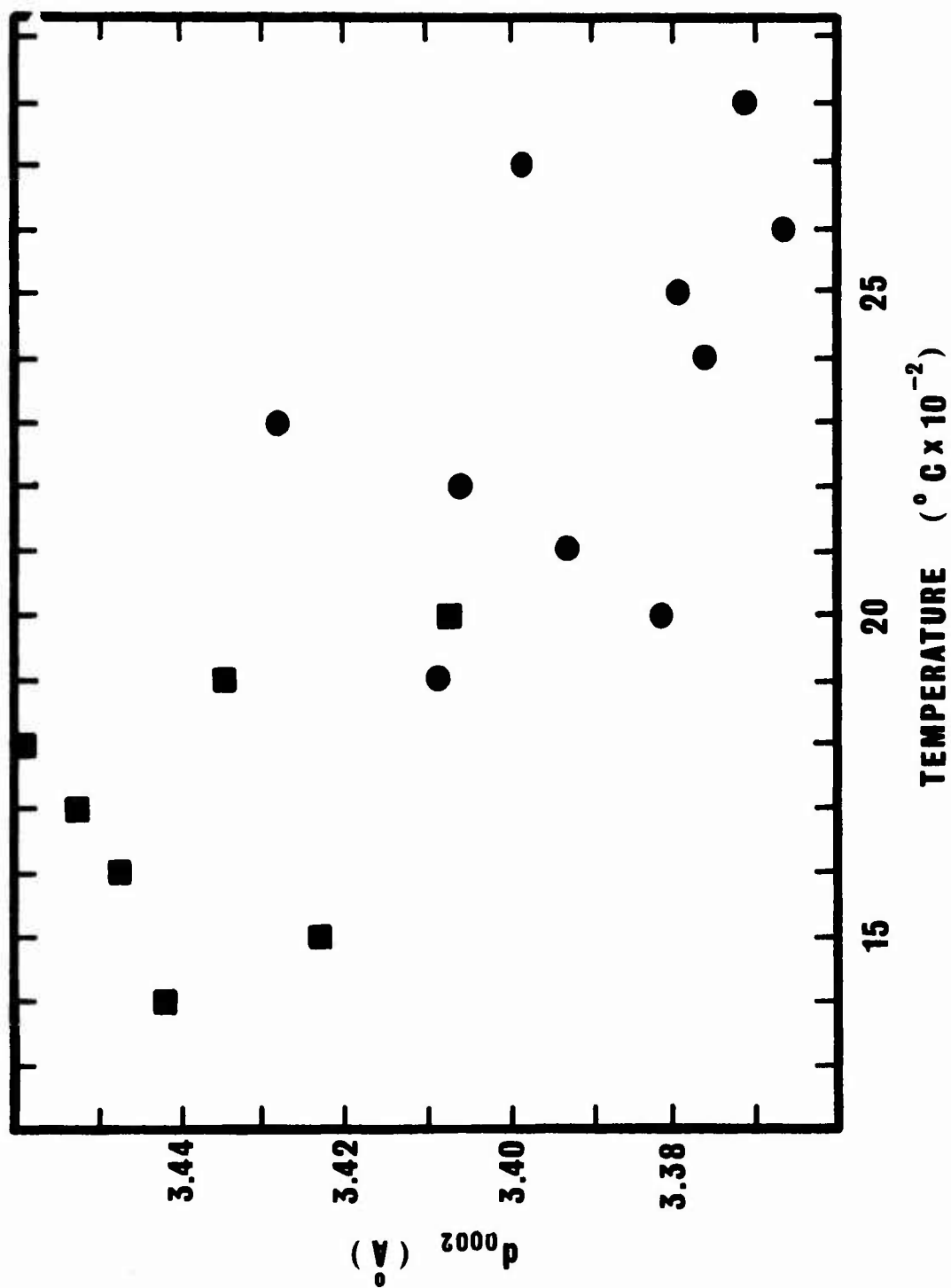


Fig. 10. Interplanar spacing ( $d_{0002}$ ) versus heat-treatment temperature for heat-treated AS carbon fibers.

to dry on an analytical balance. This permitted the recording of sample weight as a function of time as the specimen dried. The results were plotted on semi-log graph paper. It was expected that open porosity would be indicated by an initial straight line due to rapid evaporation of solvent from the bundle exterior followed by another straight line of lesser slope as the solvent evaporated more slowly from inside the pores. Of course, in the case of closed porosity, no solvent would have entered the pores and hence the initial straight line would continue until the solvent had completely evaporated from the surface.

The graphical results (Figs. 11 and 12) indicate that the porosity is closed; there is no evidence to suggest that any solvent entered into the pores. All the graphs have constant slope lines initially with abrupt changes to lines of zero slope when the solvent has completely evaporated from the exteriors of the fiber bundle. It might be expected that pore penetration would take longer than the two hour immersion periods used initially, however, the forty-eight hour specimens exhibit similar weight-time curves and so the porosity must be considered closed to these solvents.

#### C. Thermogravimetric Analysis

The dimensional measurements on PAN precursor carbon fibers, and the corresponding densities, indicate no weight loss occurred above the density minimum. Below the minimum, either open porosity existed or a weight loss occurred. Since the last section



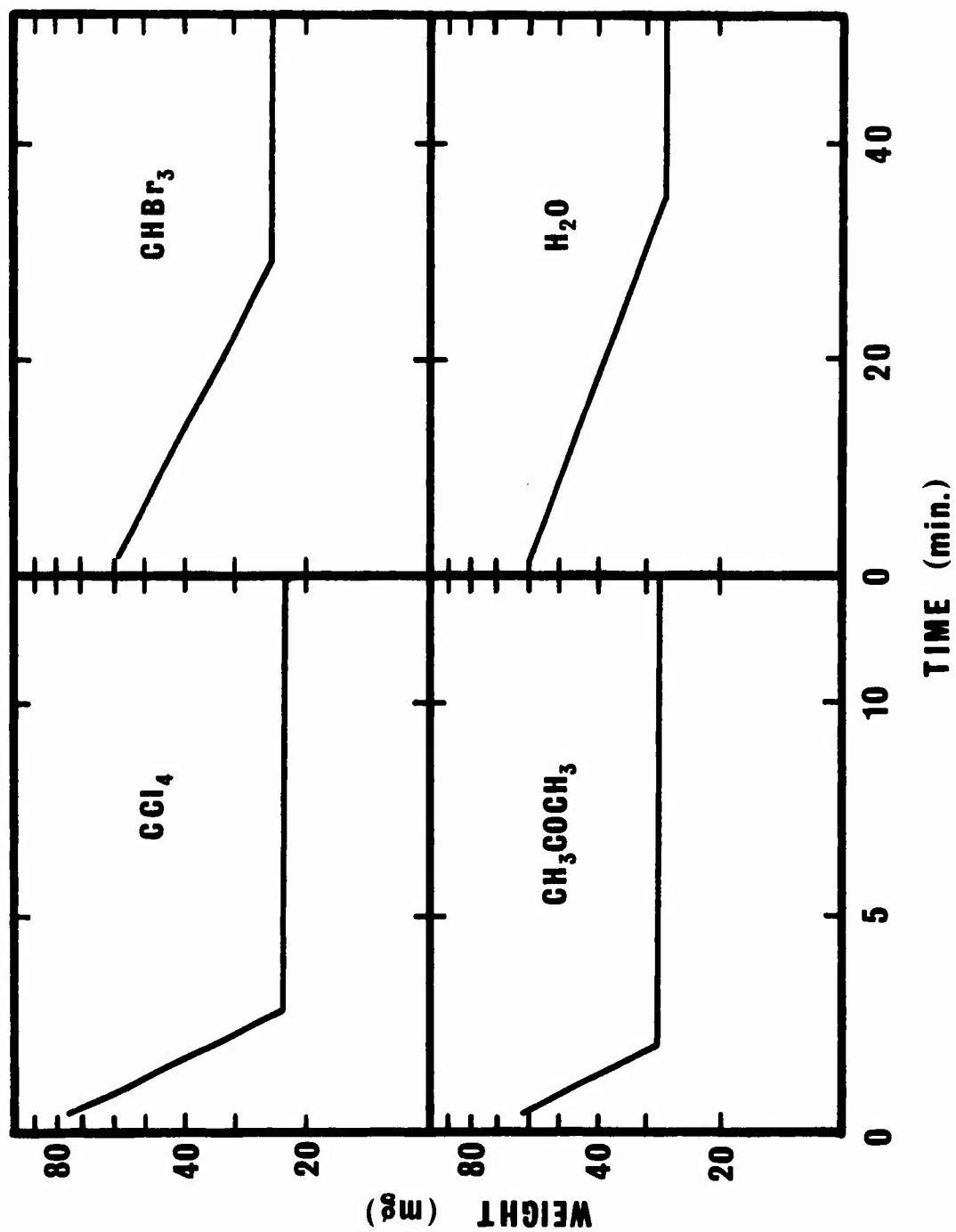


Fig. 11. Sample weight versus time for samples of HMS fiber tow immersed in various solvents (immersion time: 2 hours).

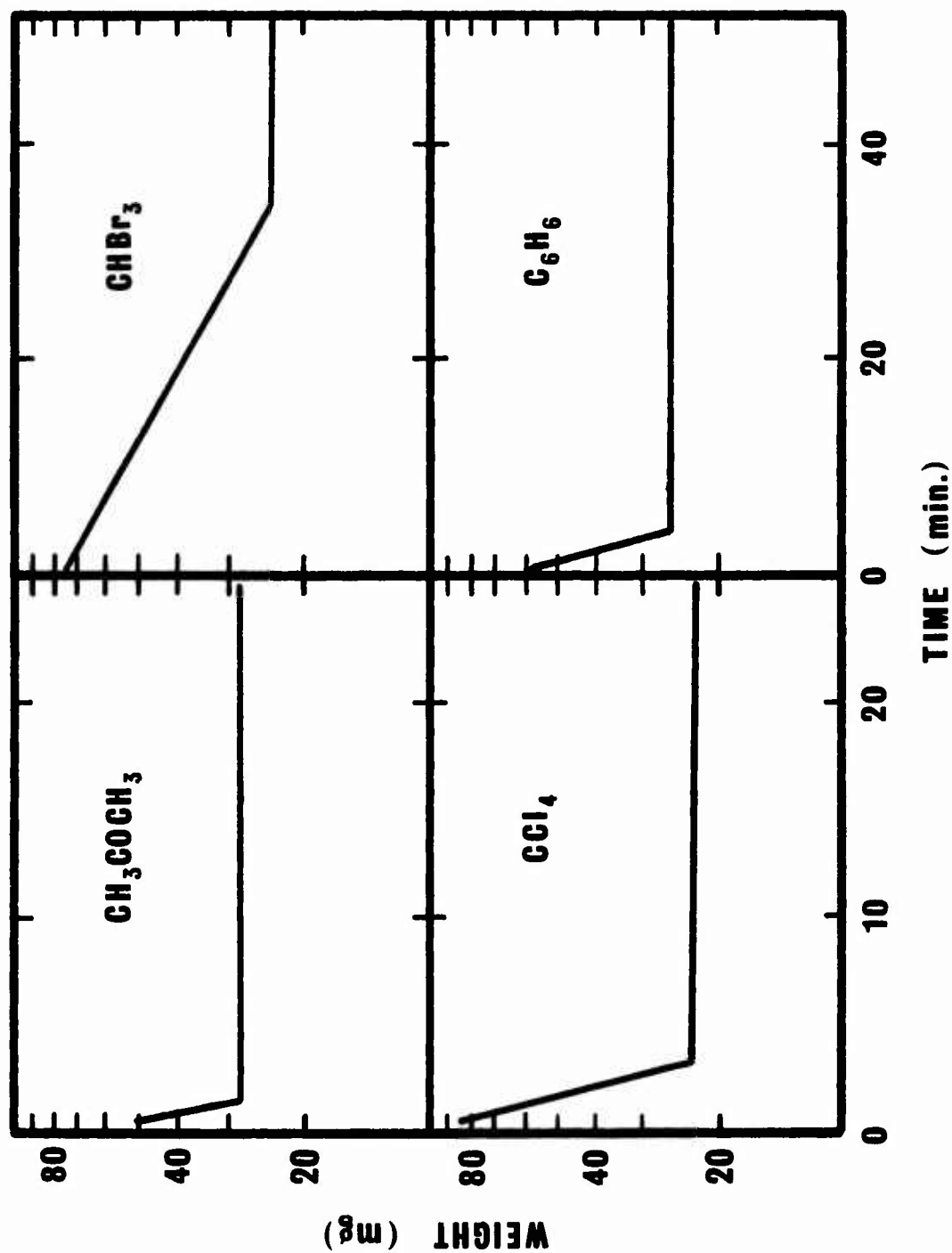


Fig. 12. Sample weight versus time for samples of HMS fiber tow immersed in various solvents (immersion time: 48 hours).

showed no evidence for open porosity, thermogravimetric analysis was used to investigate possible weight loss.

Using AS fiber, a two percent weight loss was observed between a heat-treatment temperature of 1200°C and 1700°C. This weight loss accounts for the loss in density observed in heat-treated AS fibers. Since density minima of much higher magnitude have been observed, heating rate was varied to see if weight loss was related to heating rate.

Fully stabilized Courtelle was ground to a powder in a "Wig-L-Bug" and run in a Mettler Thermoanalyser at rates of  $\frac{1}{2}$ , 2, 4, 8, 15 and 25°C/min. to 1400°C. After cool-down the powder was weighed (as a check against the TGA curve) and its density measured. The results were plotted as shown in Figs. 13 to 15.

It can be seen from Fig. 13 that slower heating rates result in a correspondingly denser final product. When the total mass lost (percentage) is plotted as a function of heating rate as in Fig. 14, it is observed that the slowest heating rates exhibit the greatest mass loss. For rates greater than 4°C/min., the weight loss was more or less constant. (It should be noted however, that the sample heated at 15°C/min. shows a mass loss value that is out of proportion to the other values. The reason for this is not clear, but probably of an experimental error in nature.)

Finally, when mass loss (percentage) is plotted as a function of temperature (to 1400°C) as in Fig. 15, a sigmoid curve results.

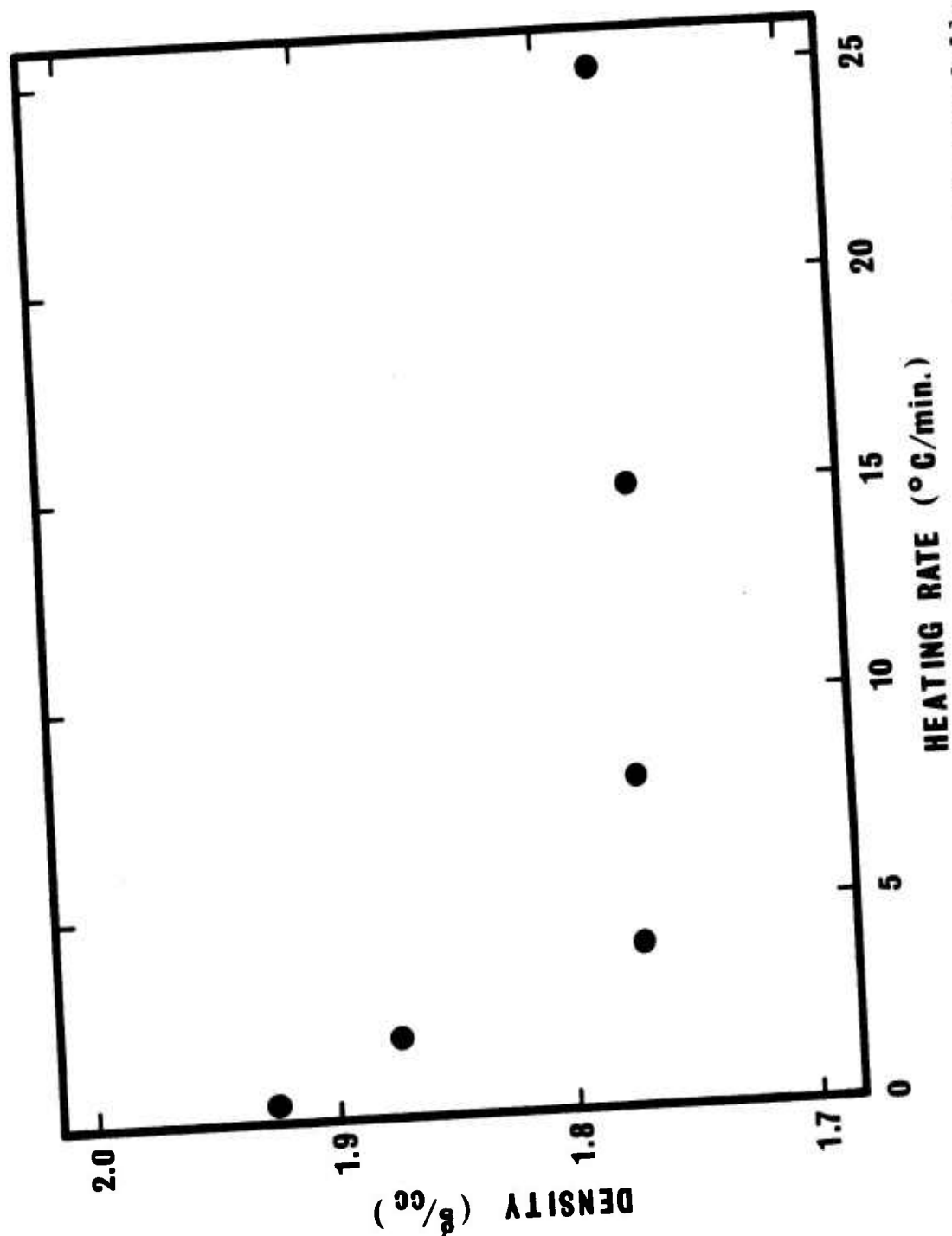


Fig. 13. Density versus heating rate of powdered samples of fully stabilized Courtelle fiber.

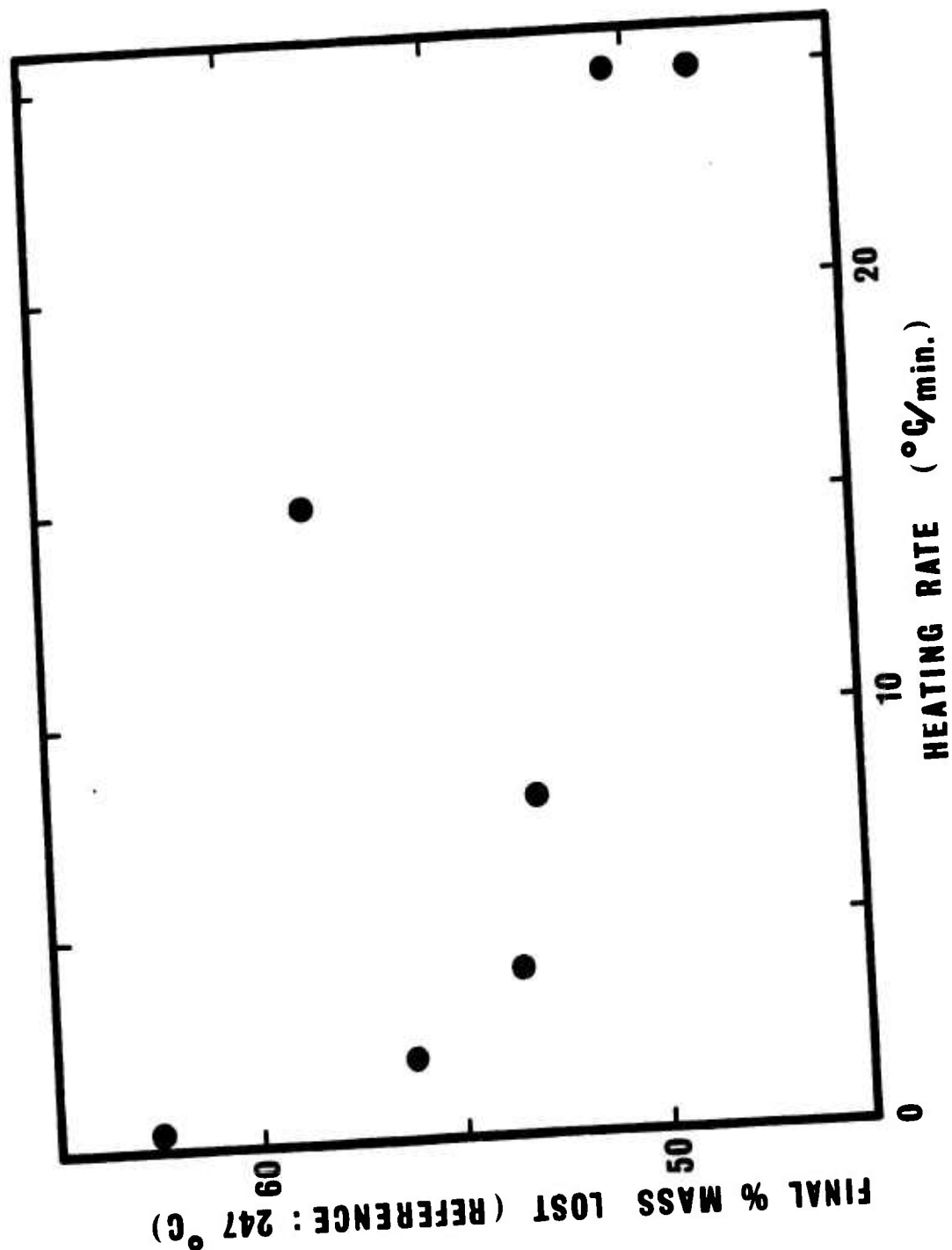


Fig. 14. Final percent mass lost versus heating rate of powdered samples of fully stabilized Courtelle fiber.

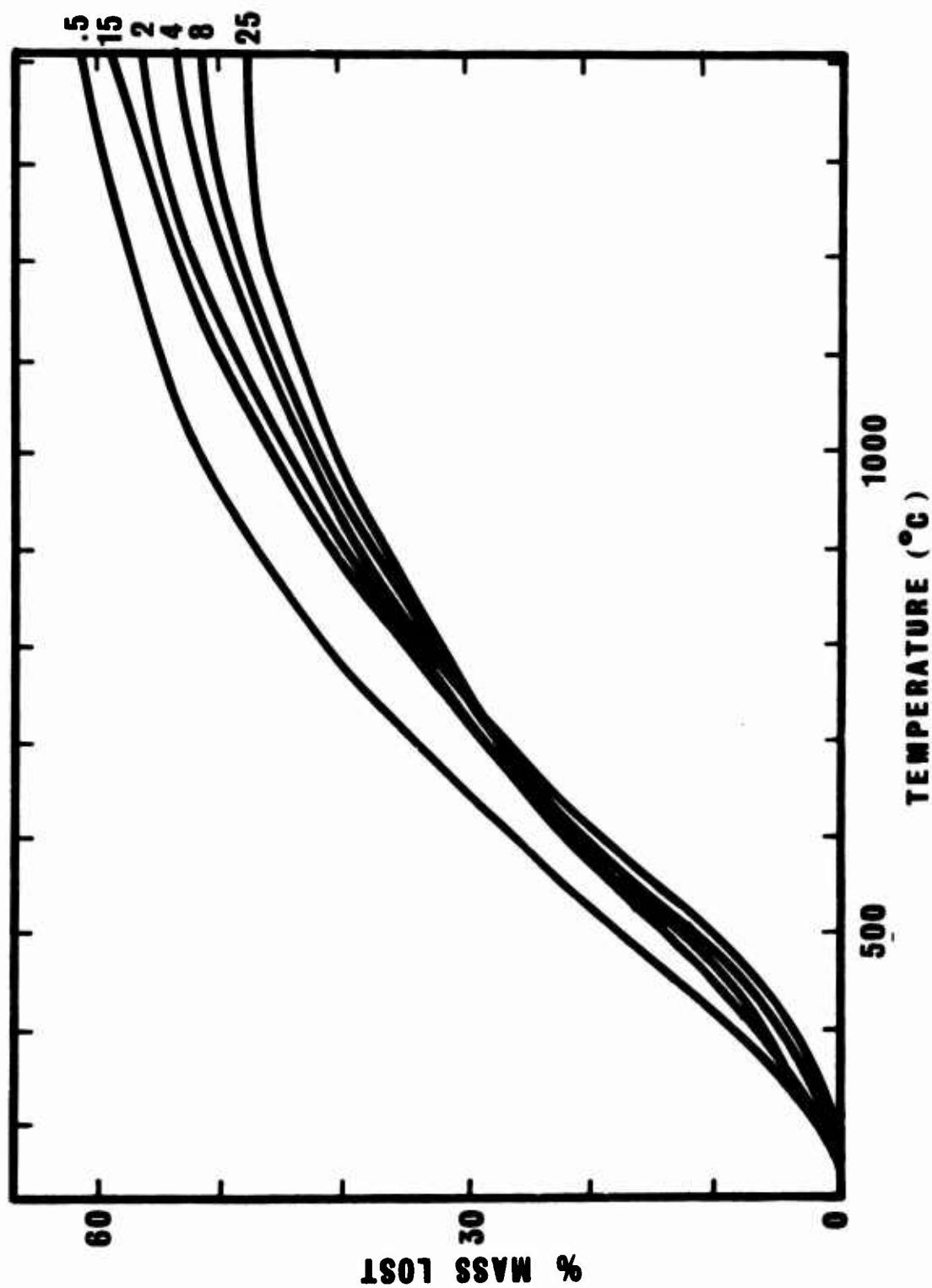


Fig. 15. Percent mass lost versus temperature for various heating rates of powdered samples of fully stabilized Courtelle fiber.

All samples, regardless of heating rate, show an initially rapid loss of mass which gradually levels off to a nearly constant value at 1400°C. The curve for the sample heated at  $\frac{1}{2}$ °C/min. shows a correspondingly higher mass loss at all temperatures, indicating a more complete rearrangement of its internal structure. Samples heated at progressively higher rates show correspondingly smaller mass losses at any given temperature. (Once again, though, the sample heated at 15°C/min. is out of sequence for reasons unknown.)

D. Homogeneity in Carbon Fiber Tows

Carbon fiber tows are generally considered to be homogeneous with respect to properties throughout the tow cross-section. The densities of portions of the total tow were measured to check on their constancy by dividing a 1 cm long bundle into 8 to 10 smaller bundles 1 cm in length. The density of each individual bundle was measured and the mean density determined. Standard deviation in bundle density was determined and is plotted versus modulus of the carbon fibers in Fig. 16. It can be seen that for carbon fibers made from Courtelle, the non-homogeneity (standard deviation) continuously increases with increasing modulus. Figure 17 is a histogram of the bundle densities.

To determine if differences in density between the interior and the exterior of the fiber tow exist, fibers were withdrawn from the center of a Great Lakes 5T tow were compared to fibers on the outside. In each case, the fibers were divided into ten approxi-

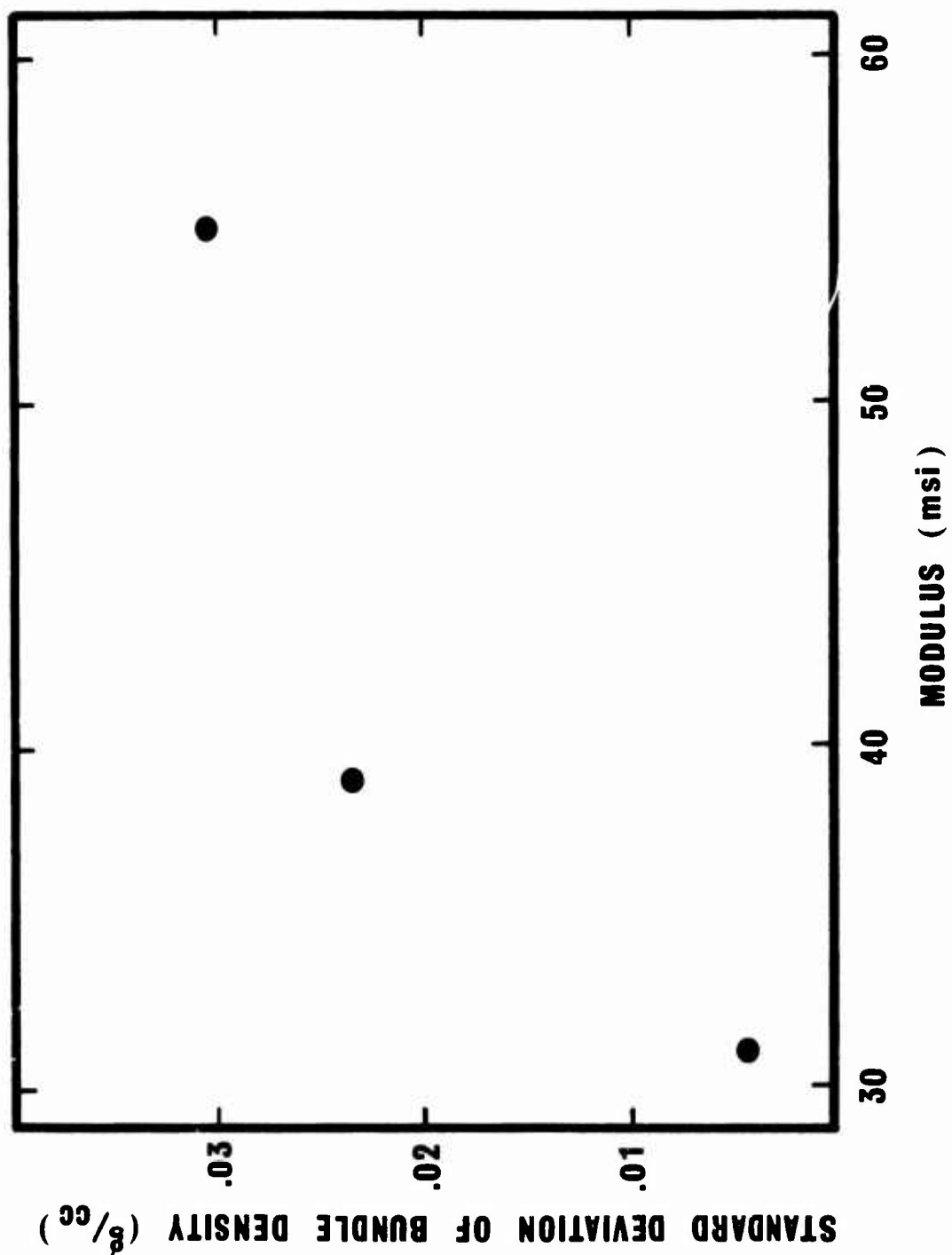


Fig. 16. Standard deviation of fiber bundle density versus carbon fiber modulus.



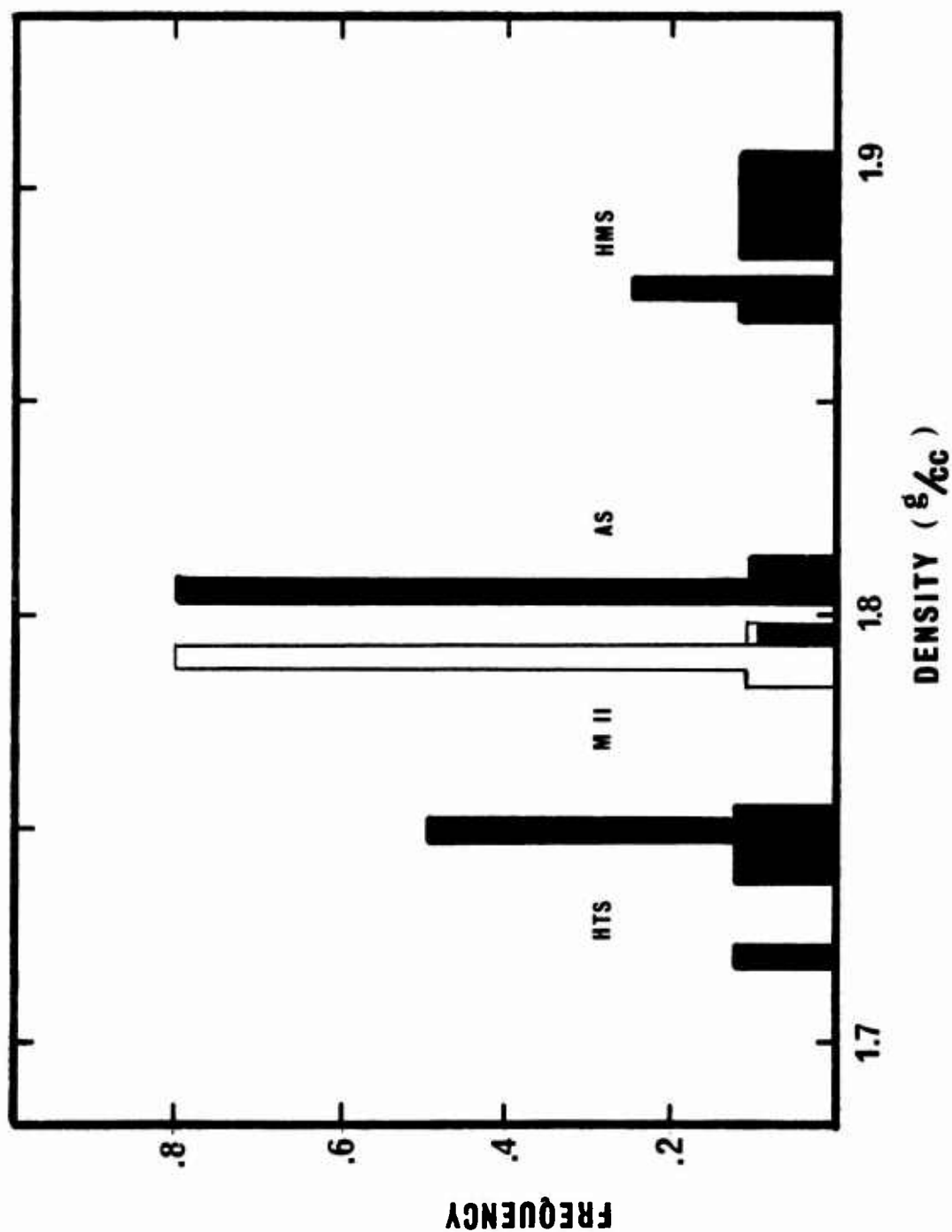


Fig. 17. Histogram showing fiber bundle density distributions for AS, HTS, HMS and Morganite II carbon fibers.

mately equal bundles, the densities measured and the means and standard deviations determined. The resulting mean was 1.902g/cc for the ten center bundles; the standard deviation was calculated to be .027g/cc with high and low bundle densities of 1.965g/cc and 1.875g/cc. For the bundles on the outside of the tow, the mean density was 1.900g/cc with a standard deviation of .005g/cc. The high and low bundle densities were 1.911g/cc and 1.895g/cc. Clearly, the exterior fibers of the tow appear to have a much more uniform density than the central tow fibers (the difference in the variances is highly significant, i.e. not due to random error when a standard F-test is used for variance comparison).

#### E. Conclusions

A minimum in density is observed for PAN precursor fibers with increasing heat-treatment. The minimum is not caused by changes in open porosity, nor by a length increase caused by the straightening of the undulating graphite ribbons. Apparently the expected increase in length is inhibited, perhaps by the decrease in preferred orientation from the surface to the core of the fiber. (The highly ordered skin which is observed in these fibers would resist elongation.) The initial decrease in density is caused by weight loss, while the subsequent increase is a result of dimensional changes. The precise shape of the density curve is affected by heating rate.

Finally, some evidence indicates non-homogeneity in properties across the cross-section of heavy tows.

### SECTION III

#### MODES OF FAILURE IN KEVLAR I, III, IV AND FIBER B

These organic fibers are essentially arrays of parapolybenzamide or similar polymers parallel to the fiber axis. Hydrogen bonding results in a crystalline planar structure rather similar to graphite. These fibers are stable under tensile stress but buckling occurs in compression. This buckling manifests itself as oblique microscopic strain markings. Since buckling is essentially a shearing phenomena, any yielding which occurs (strain bands) will be along the direction of maximum shear stress. A more poorly oriented array of molecules might be relatively stable in compression due to the restraint the molecules place on each other. However, the poorly oriented fiber when stressed in tension would show a large increase in orientation, thus reducing the fiber diameter, or more likely with these type polymers, open up voids. Obviously, this would badly degrade tensile properties.

Crimped specimens of fiber B, Kevlar I, III and IV were examined and photographed under polarized light. Fiber B exhibited oblique strain bands only at the crimp. Many transverse strain bands were found along the fiber in directions away from the crimp. This suggests, as discussed above, that fiber B has a more poorly oriented array of long molecules comprising its bulk. Kevlar III and IV showed oblique strain markings not only at the crimp site but in both directions beyond the crimp. The markings seemed to

spiral down the length of the fiber. Transverse tensile strain markings were rarely observed. Kevlar I exhibited very distinct, spiraling, oblique strain markings at the crimp and in both directions away from the crimp. No transverse strain markings were observed. Fracture was observed in this fiber when crimped an amount less than that of Kevlar III, suggesting that Kevlar I is composed of very highly oriented individual molecules with little interaction amongst them. Due to the absence of transverse strain markings, it would seem that the tensile stress associated with the compressive stresses during bending of the fiber have little or no effect upon it. All these observations are consistent with X-ray preferred orientation measurements which show PRD-49-I most ordered and fiber B least ordered.

#### SECTION IV

##### ABRASION AND FIBER STRENGTH

###### A. Experimental

A small number of AS specimens were tested to give an indication of whether or not the abrasion effect is large. The specimens were tested using a one-inch gauge length dry fiber technique. Although it is easier to test a single dry fiber, it was felt that abrading and testing a tow would give cumulative failures to break. The major difficulty encountered was gripping the ends of the specimen. Ideally, individual fibers in the fiber tow would break in random places along the gauge length; in reality, it was found

that specimens in which pull-out from the grip did not occur generally failed at or near the grip itself. The technique finally used for the specimens tested could, had time permitted, probably have been improved to give higher reliability in obtaining satisfactory specimen failure. A schematic diagram of the specimens used is shown in Fig. 18.

The control specimens, i.e., the non-abraded ones were handled with as much care as possible so that once the sample tow was removed from the spool, the gauge length section was virtually untouched by any other body. For the other specimens, abrasion consisted of placing the tows on a flat glass plate and rolling a stainless steel cylindrical weight ( $\approx 360\text{g}$ ) back and forth over the central one-half inch of the length. It was thought that if this abrasion was significant, the samples would tend to fracture in the central region of the tow in addition to exhibiting lower strengths. The specimens were tested in an Instron at a constant strain rate.

Abraded and non-abraded specimens were observed under the light microscope to see if there was any evidence of introduced flaws.

## B. Results and Discussion

The resulting ultimate tensile loads are shown in Table 1. Although based on very few results, the abraded specimens did not exhibit a drastically lower tensile strength compared to the non-

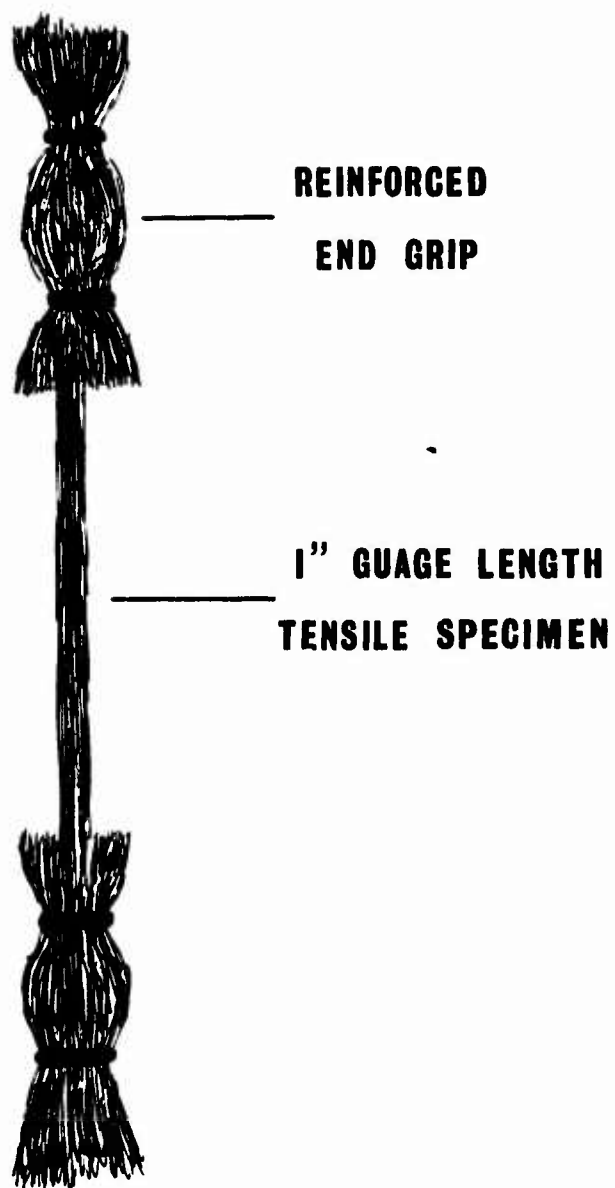


Fig. 18. Schematic diagram of tensile test fiber tow specimens.

Table 1  
MAXIMUM TENSILE LOADS OBTAINED WITH ABRADED  
AND "UNABRADED" AS FIBER TOWS

<u>Unabraded</u>	<u>Abraded</u>
Specimen Designation	Specimen Designation
AS-(a) 156 lb.	AS-(b) 126 lb.
AS-(d) 151 lb.(pull-out)	AS-(c) 158 lb.
	AS-(e) 135 lb.(pull-out)
	AS-(f) 126 lb.(pull-out)

abraded ones. Also, there seemed to be no particular preference in the abraded specimens for failure near the center of the gauge length as would be expected if the abrasion had substantially weakened the tow. Of course, these few results are not sufficient to define precisely the effect of the abrasion however, it would appear that either the abrasion was not severe enough or, that the existing flaws in the tow were sufficient to weaken the tow so that introduction of more defects by abrasion did not have much effect.

There was little difference optically between non-abraded and severely abraded specimens. Severe abrasion was produced by "scrubbing" the fibers between a glass microscope slide and a cover slide. The severe abrasion caused much fiber breakage but there were no obvious flaws present in the abraded fibers at 400X magnification. This would seem to indicate that any flaws introduced are beyond the resolution power of the optical microscope.

#### C. Conclusions

1) Since the abraded specimens did not indicate a drastic reduction in strength or a propensity for failure in the abraded section of the gauge length, either the abrasion did not cause significant flaw damage or the flaws introduced did not substantially increase the flaw concentration.

2) Rough handling of carbon fibers during prepregging or composite fabrication probably does not decrease composite properties



drastically. However, improved handling during fiber production might decrease flaws, and increase strength, but make the fiber sensitive to subsequent handling.

3) Fiber breakage was the only optical indication of severe abrasion; any flaws introduced were probably beyond the resolution of the optical microscope.

## SECTION V

### COMPARISON OF CCA-1 RAYON PRECURSOR CARBON FIBER AND ITS REPLACEMENTS

There have been differences in composite behavior using CCA-1, CCA-2 and CCA-2-10 carbon fibers. Since these fibers were hopefully equivalent, the reasons for these differences were investigated. Samples of CCA-1, CCA-2 and CCA-2-10 as well as their respective precursors: IRC, old ENKA and new ENKA rayons were analysed for optical microstructure, differential thermal analysis (DTA) and thermo-gravimetric analysis (TGA). Also, X-ray analysis was carried out on the CCA-1 and CCA-2 samples.

#### A. Experimental

Specimens of each of the precursor rayon and carbon fibers were mounted carefully in epoxy so that the fiber bundles would be parallel to the incoming light beam. Conventional grinding and polishing (to .05 $\mu$  alumina) were used to prepare the samples for optical observation using plain and polarized light.

Bulk X-ray diffraction data was used to generate  $d_{0002}$  (interplanar spacing) and  $l_c$  (crystallite sizes) values for the

IRC-based graphite fiber cloth (CCA-1) and old ENKA-based cloth (CCA-2).

Thermal analysis was performed using a Mettler Thermoanalyser. Samples of the CCA's of from 50-100mg were pulverized in a "Wig-L-Bug"; it was not possible to pulverize the rayons. Powdered HMS carbon fiber was used as the reference since its high heat-treatment temperature rendered it least likely to undergo further microstructural change upon heating to 1600°C. Argon at a constant rate of flow was used as the atmosphere over the samples. A constant heating rate of 8°C/min. up to 1600°C was used to obtain temperature weight and DTA curves.

#### B. Observations and Discussion

Photomicrographs of the rayon and CCA specimens are shown in Figs. 19 and 20 respectively. No polarized light pictures are included as there was no visible optical activity in any of the rayons and little in the CCA's. What optical activity that did exist in the CCA's appeared to be the same for all specimens.

Although the rayons are of essentially the same average diameter, old ENKA has a more crenulated surface than either of the IRC or new ENKA rayons, i.e. the axial grooves tend to extend deeper into the old ENKA fiber. The polished cross-sections of all the fibers tend to be smooth with no visible surface relief.

The CCA's are also similar in terms of cross-sectional size and shape. The polished cross-sections, although quite smooth

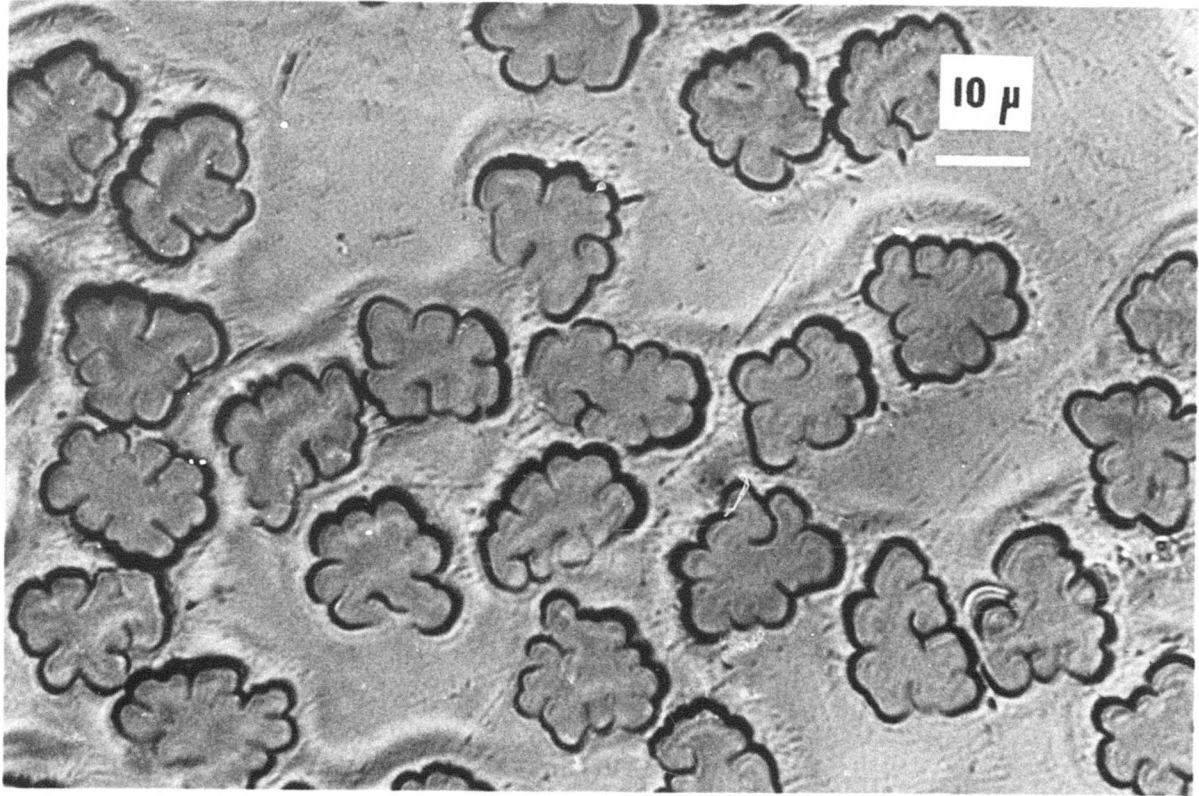
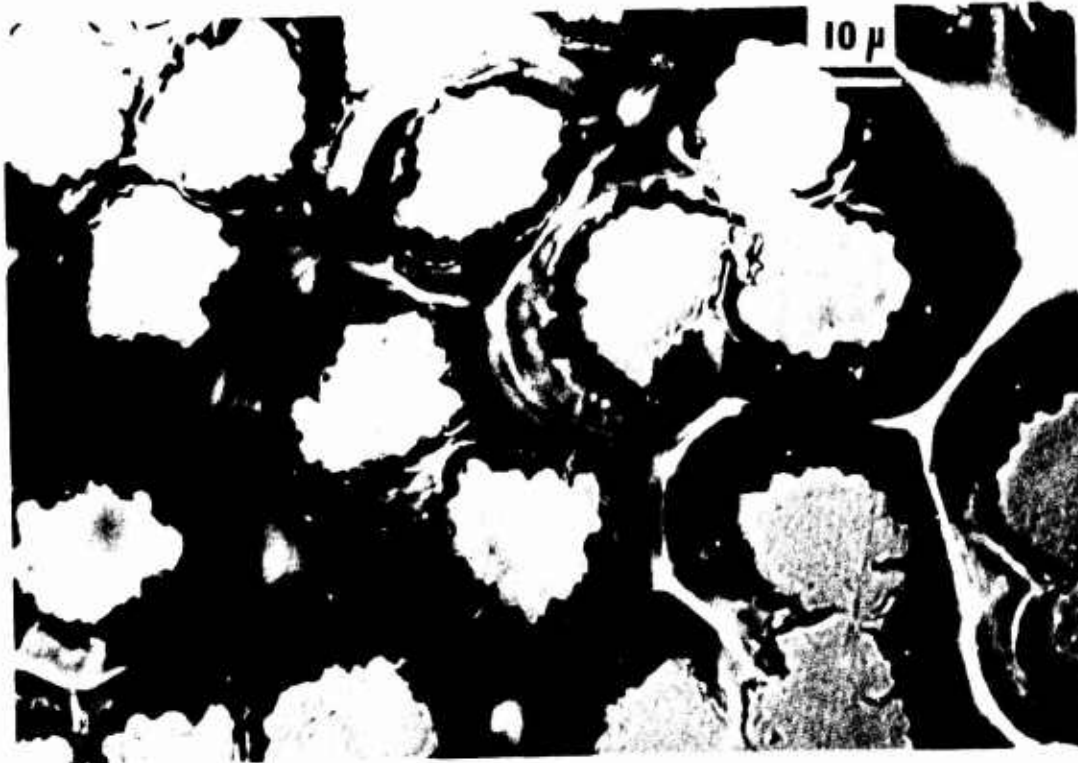


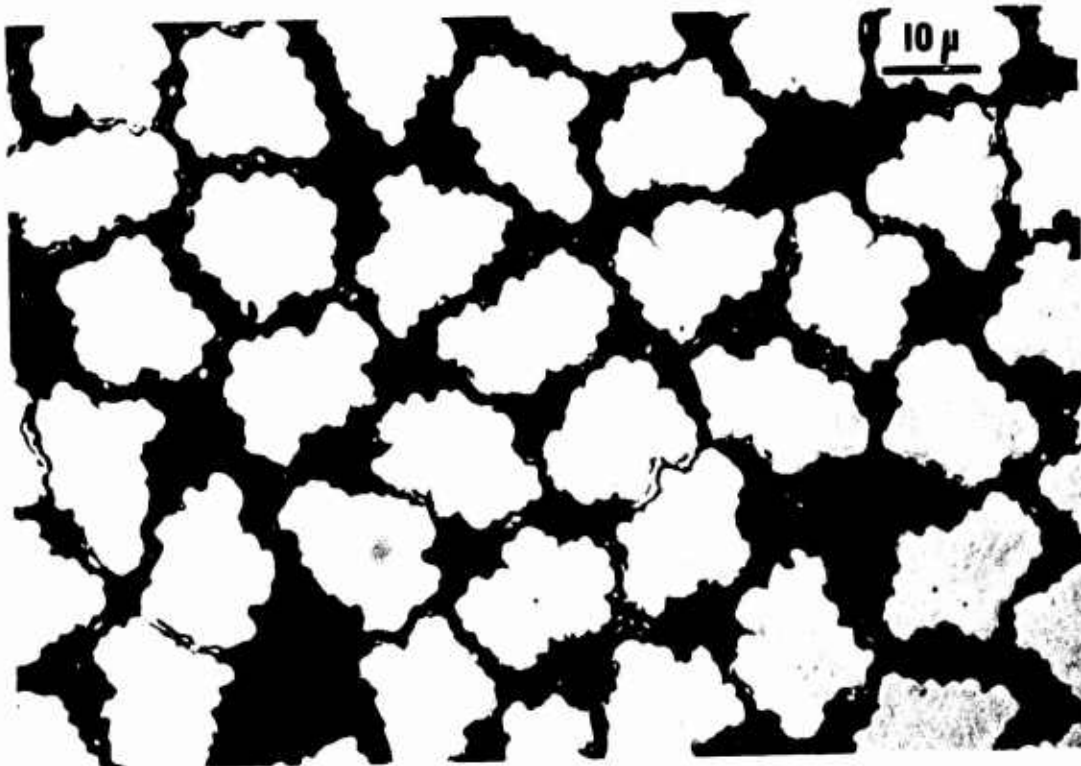
Figure 19

Optical Micrographs of Rayon Precursors  
Mounted in Epoxy

a) "Old" ENKA Rayon



(a)



(b)

Figure 19

- b) "New" ENKA Rayon
- c) IRC Rayon

illustrate an important distinction between CCA-1 and the CCA-2's: surface "pitting" of the fibers is evident in both CCA-2 and CCA-2-1614-10 but not in CCA-1. This pitting is probably evidence of a difference in porosity between the two types of fibers. The  $d_{0002}$  and  $l_c$  values are given below:

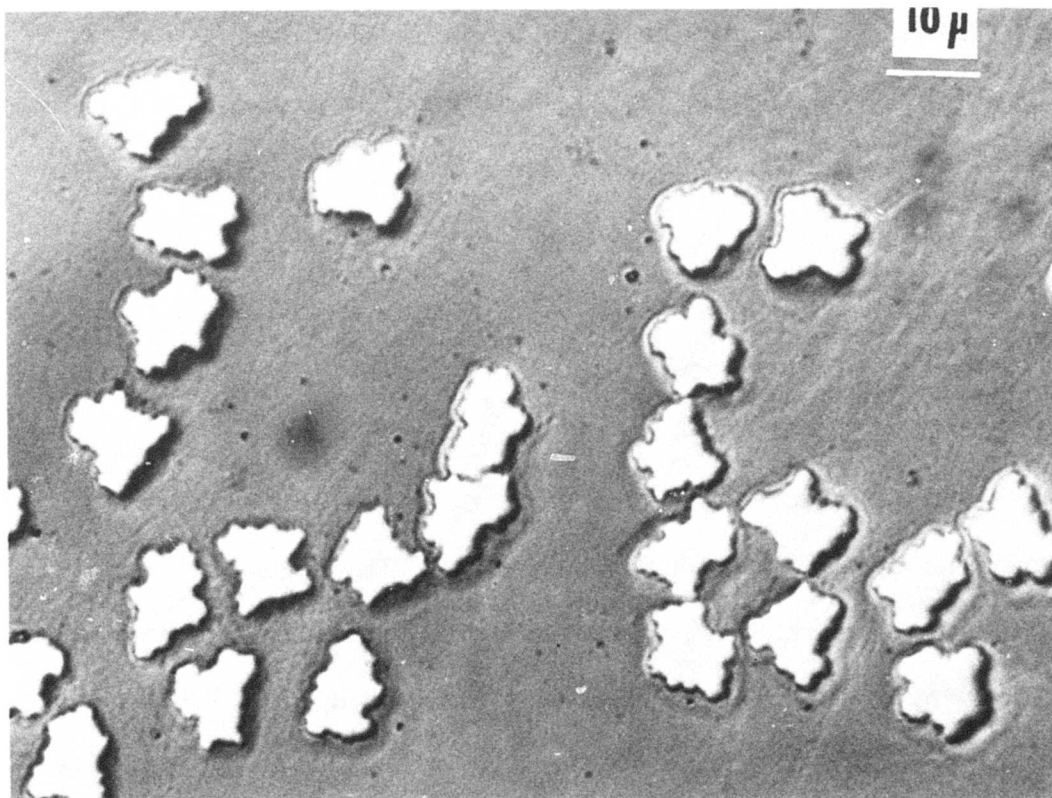
	$d_{0002}$	$l_c$
CCA-1	3.5Å	45Å
CCA-2	3.49Å	48Å

Thus, CCA-1 and CCA-2 are almost identical in these parameters.

Thermal analysis data is shown in Figs. 21 and 22 for the rayon precursors and in Figs. 23 to 25 for the CCA carbon fiber cloths.

The percent weight as a function of thermocouple voltage and converted temperature is shown in Fig. 26 for old and new ENKA as well as IRC rayons. The curves are generally similar in shape with an initial weight loss (due to release of water) followed by a plateau up to almost 300°C. Above this temperature, there is a large and rapid weight loss as the rayons are carbonized. This tapers off at 600°C, above which temperature, the weight loss is fairly linear for all three rayons.

The weight loss curves for old and new ENKA are virtually coincident throughout most of the temperature range. The IRC curve is somewhat further removed particularly at the upper end of the scale where the weight loss with increasing temperature is considerably less than that for the other rayons. This would

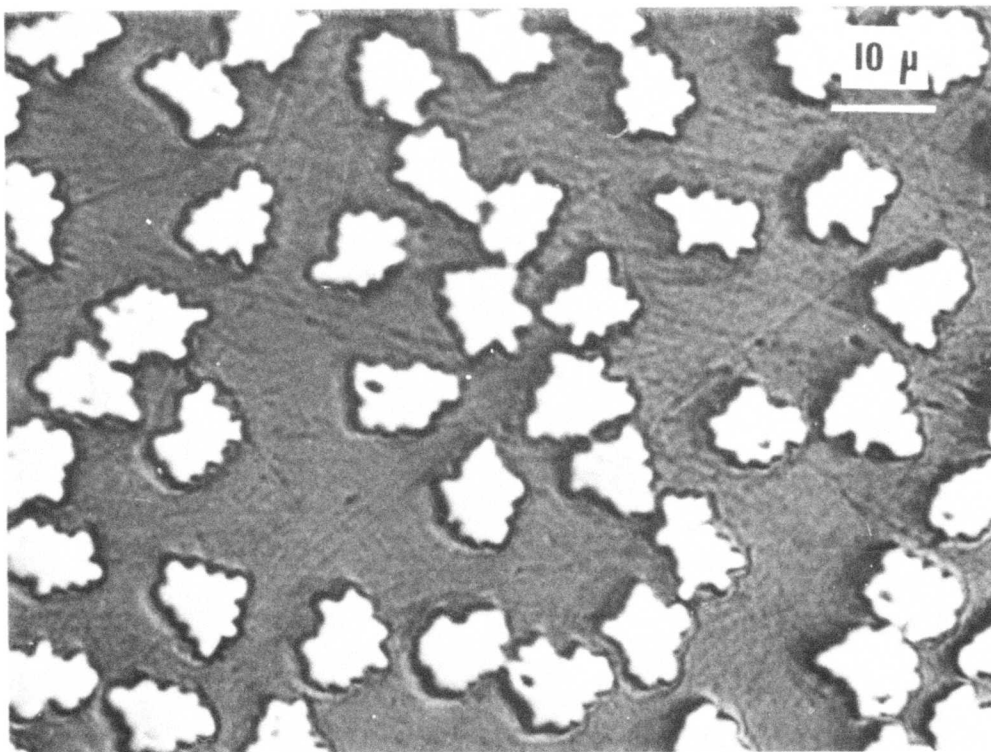


(a)

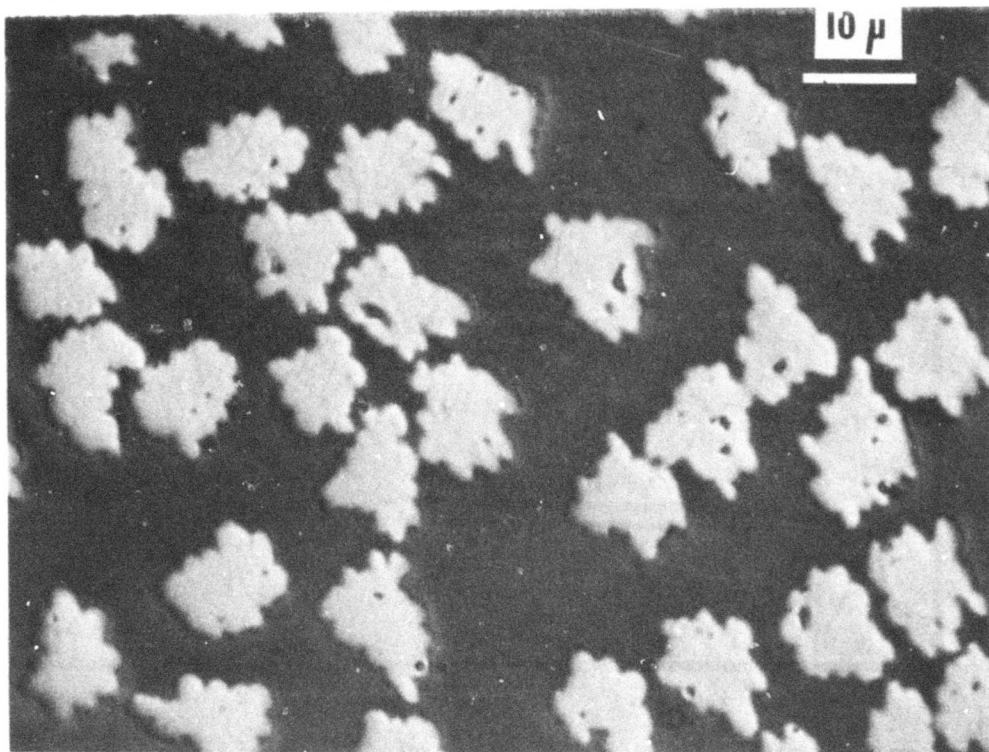
Figure 20

Optical Micrographs of Carbon Fibers From  
Rayon Precursors Mounted in Epoxy

a) CCA-1



(b)



(c)

Figure 20

b) CCA-2

c) CCA-2-1641-10

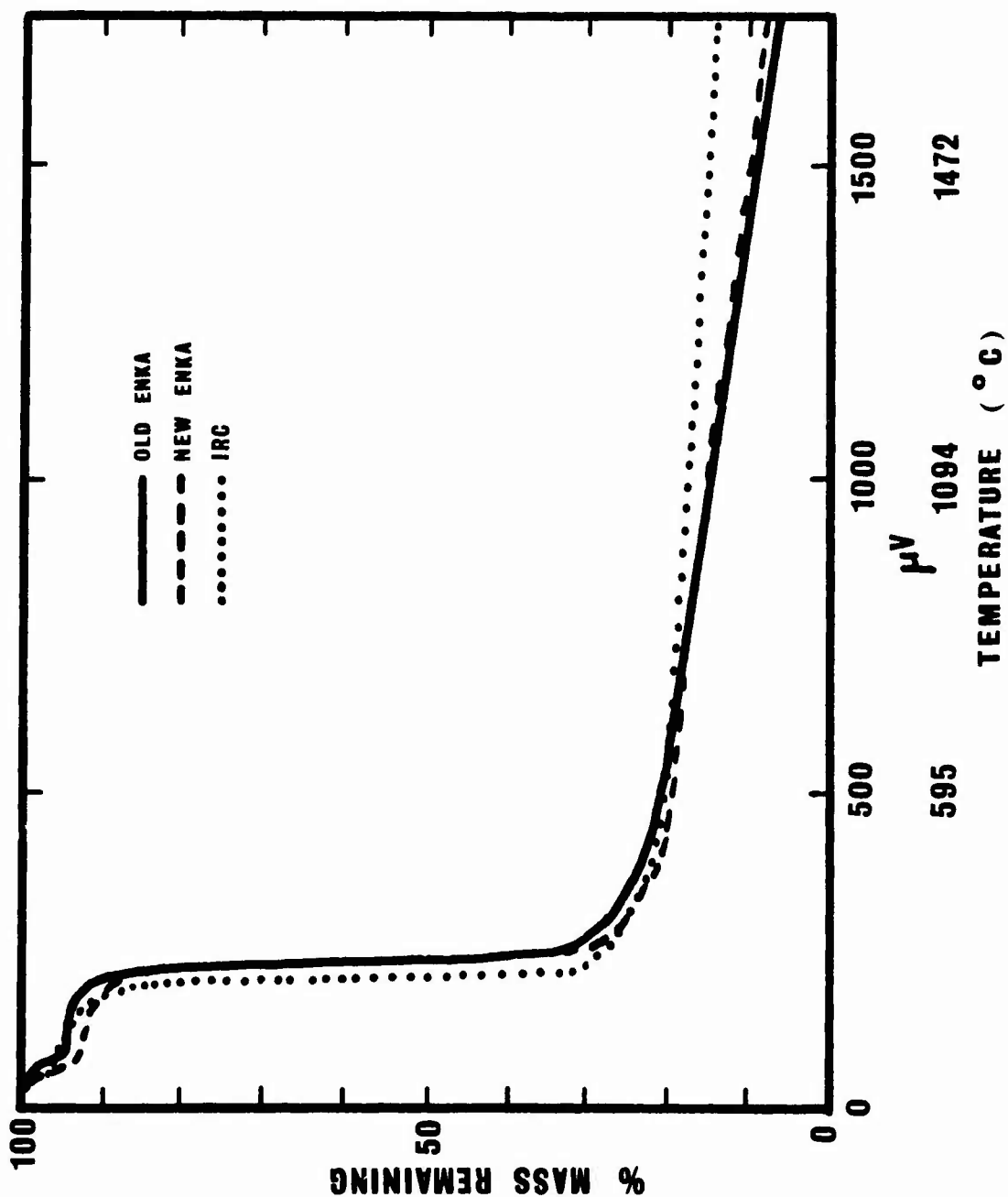


Fig. 21. Percent mass remaining versus thermocouple voltage and corresponding temperature for three rayon fibers.



seem to indicate that the carbon fiber yield from IRC rayon would be substantially higher than either of the ENKA rayons, at least at these heating rates.

The DTA curves for the rayons are shown in Fig. 22. Apart from amplitude differences, the curves for all three rayons decrease up to about 600°C after which there is a smooth gradual increase up to 1600°C with the exception of an anomaly at about 960-970°C. This sudden drop is evident in all three curves but is most pronounced in that for new ENKA rayon. The reason for this discontinuity is unknown and at the time there was insufficient new ENKA rayon for a reproducibility test to confirm this observation. The most likely explanation is a machine error.

Actual thermoanalyser traces are shown in Figs. 23 to 25 for CCA-1, CCA-2 and CCA-2-1614-10 carbon cloths respectively. The weight trace for CCA-1 is distinctly different from the other two. The final weight loss is small (only about 4% compared to over 15% loss for CCA-2). Also, there is no evidence of the rapid initial drop in weight around 100°C as occurs in CCA-2 and CCA-2-1614-10. In fact, there is a slight weight increase (reaching a maximum of + 0.25%) from room temperature to about 270°C which is caused by buoyancy effects. Also, the initial weight loss due to water is much smaller in CCA-2-1614-10 than in CCA-2.

The DTA curves for the CCA-2's are quite similar with the exception of the strong high temperature exotherms. The curve for

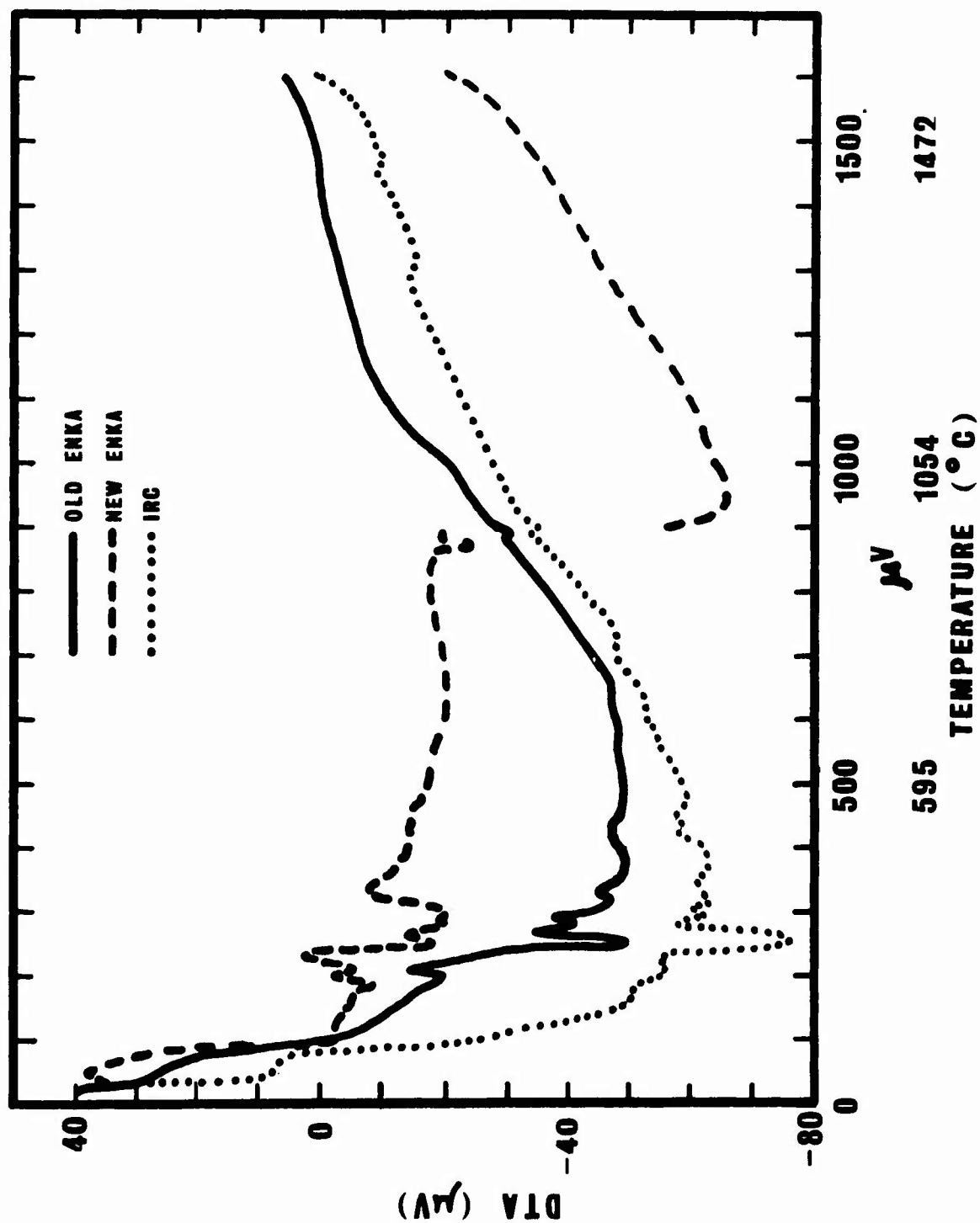


Fig. 22. DTA (difference in thermocouple voltage) versus thermocou voltage and temperature for three rayon fibers.

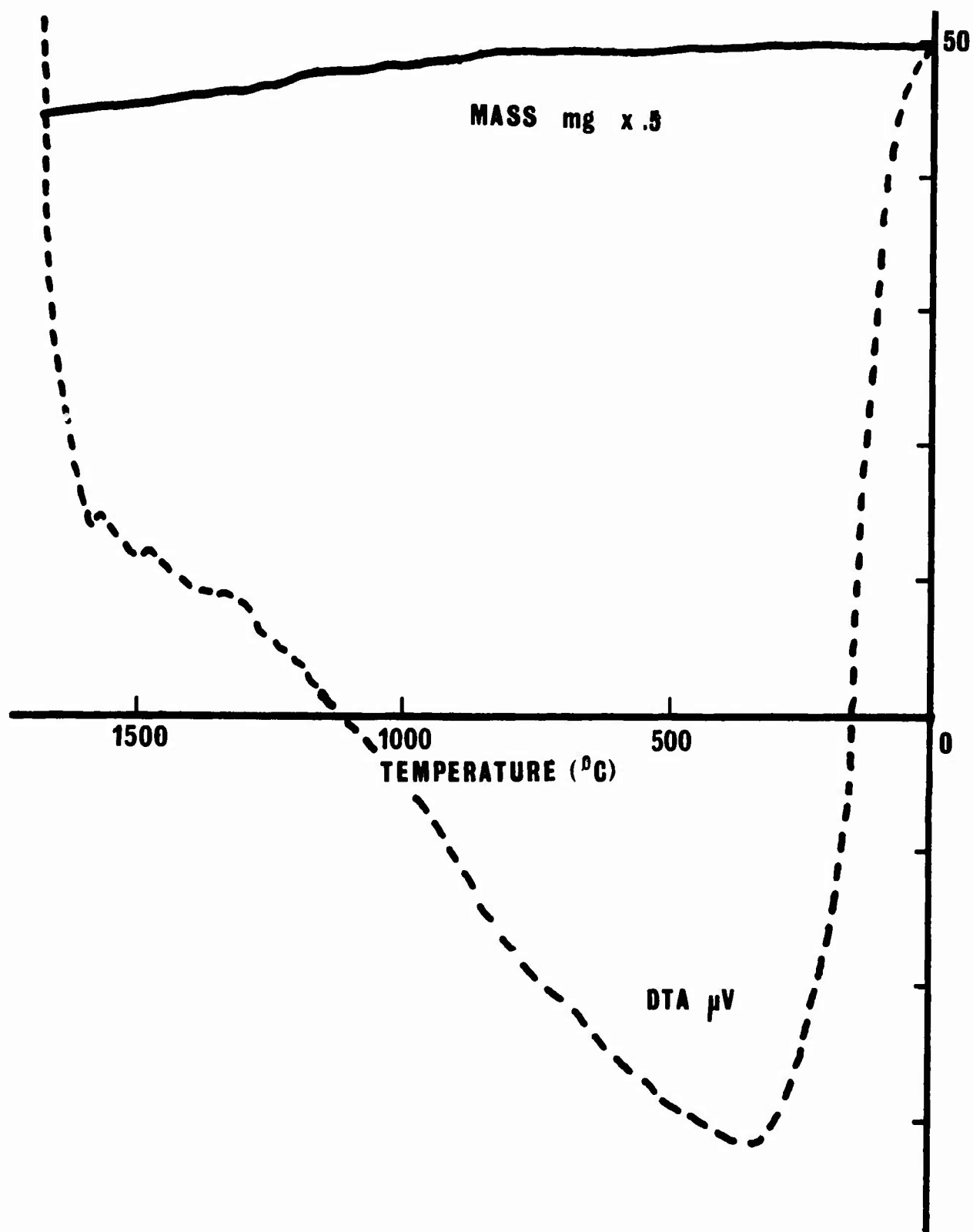


Figure 23  
Thermoanalyser Trace for CCA-1 Carbon Fiber  
(Heating rate" 8°C/min.)

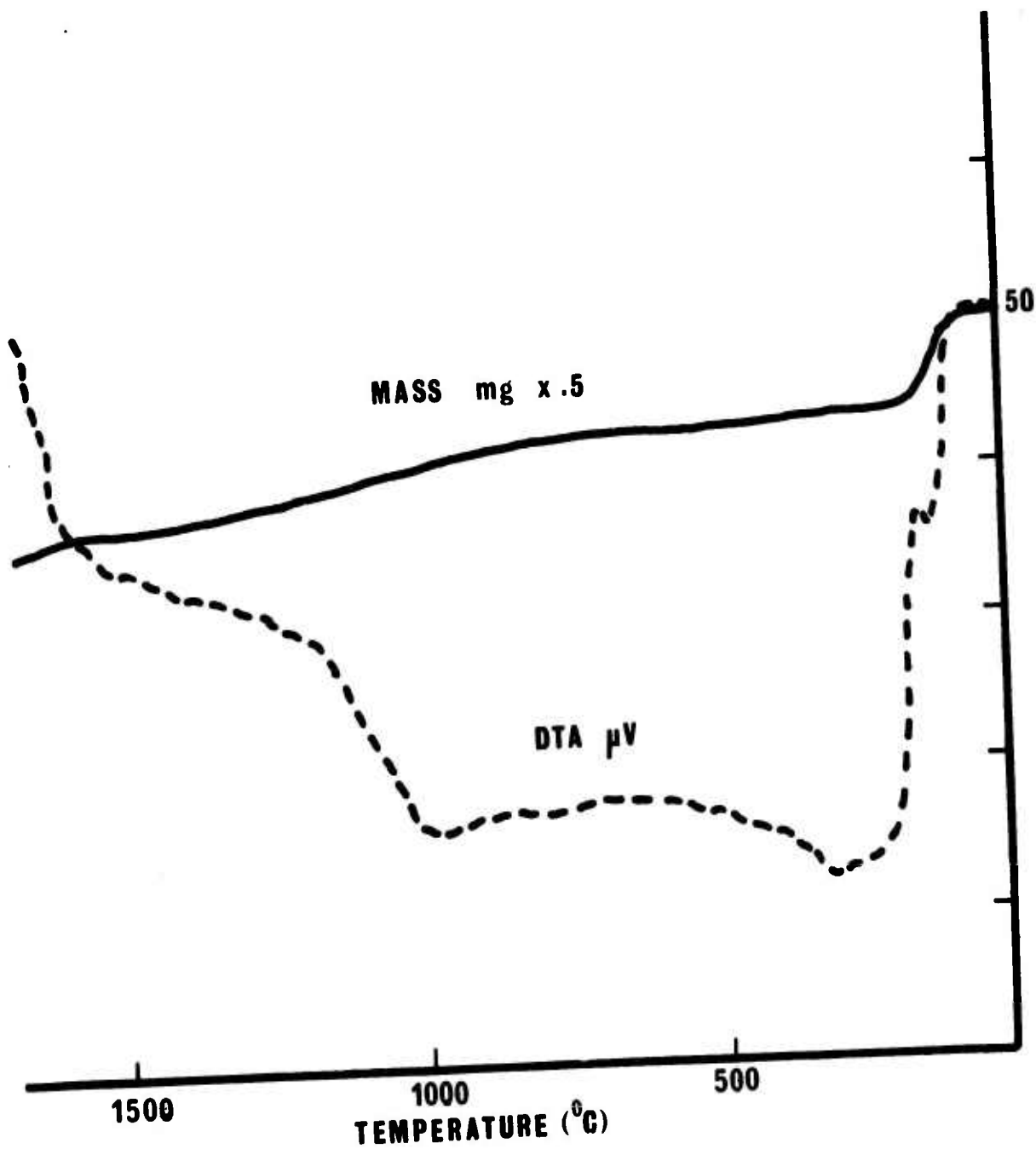


Figure 24  
Thermal Analyser Trace for CCA-2 Carbon Fiber.  
(Heating rate:  $8^{\circ}\text{C}/\text{min.}$ )

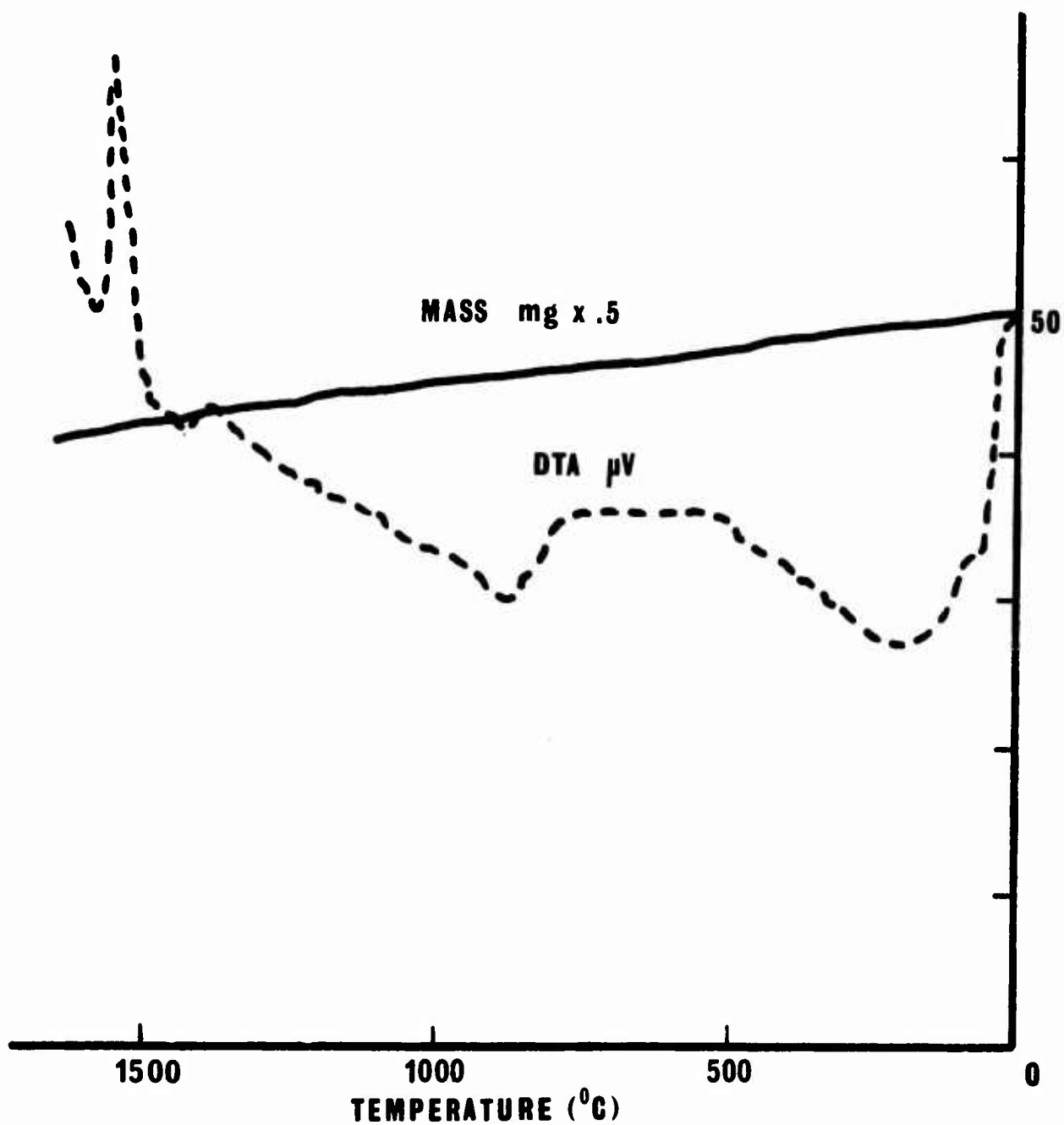


Figure 25

Thermal Analyser Trace for CCA-2-1641-10 Carbon Fiber.  
(Heating rate: 8 $^{\circ}$ C/min.)

CCA-1 is also rather similar except that the endotherm at intermediate temperatures. The sources for the exo- and endotherms are not known.

### C. Conclusions

It can be generally concluded that the carbon fiber cloths and their rayon precursors are different in many respects and these differences can be expected to result in performance changes (specifically mechanical) in applications where the original CCA-1 is replaced by either of the two newer substitutes.

As well, the following specific conclusions can be made on a basis of experimentation described:

1) The two ENKA rayon precursors are fairly similar in terms of thermal analysis characteristics and differ substantially from the IRC specimen.

2) The rayons are microstructurally similar apart from the more deeply crenulated surface of the old ENKA fiber.

3) The cross-sectional surface of the CCA-2 fibers exhibit a pitted surface (evidence of internal porosity) in contrast to the smooth surface of CCA-1.

4) The weight loss curve for CCA-1 is different from those for CCA-2's. Part of this difference is due to adsorbed water but at higher temperatures it may be caused by higher adsorption of oxygen which desorbs as CO and CO<sub>2</sub>. Both indicate higher porosity in the CCA-2's as was suggested by the pitting of the microstructure.

A comparison of CCA-2 with CCA-2-10 indicates that the latter has appreciably less absorbed water. If absorbed water is deleterious, the performance of the fibers should be (in decreasing order): CCA-1, CCA-2-10, CCA-2. Obviously, the CCA-2's could be vacuum degassed at moderate temperatures to eliminate water. It is our experience that after an initial degassing, the magnitude of water pickup is reduced. However, degassing may solve a short-term problem but replace it with a problem which appears after many months.

## SECTION VI

### MICROSTRUCTURE OF PITCH-BASED CARBON FIBERS

#### A. Experimental

Two samples of Union Carbide pitch-based carbon fibers were provided for examination. Both types (hereafter referred to as "Pitch I" and Pitch II") were discontinuous and in mat form. Moduli supplied by the manufacturer were 85msi and 20-30msi for I and II respectively. The fibers in the mats were relatively short (about 3/16 inch for Pitch I and about one inch for Pitch II). Samples of the fibers were aligned and then mounted in epoxy for observation. Average densities for both mats were determined.

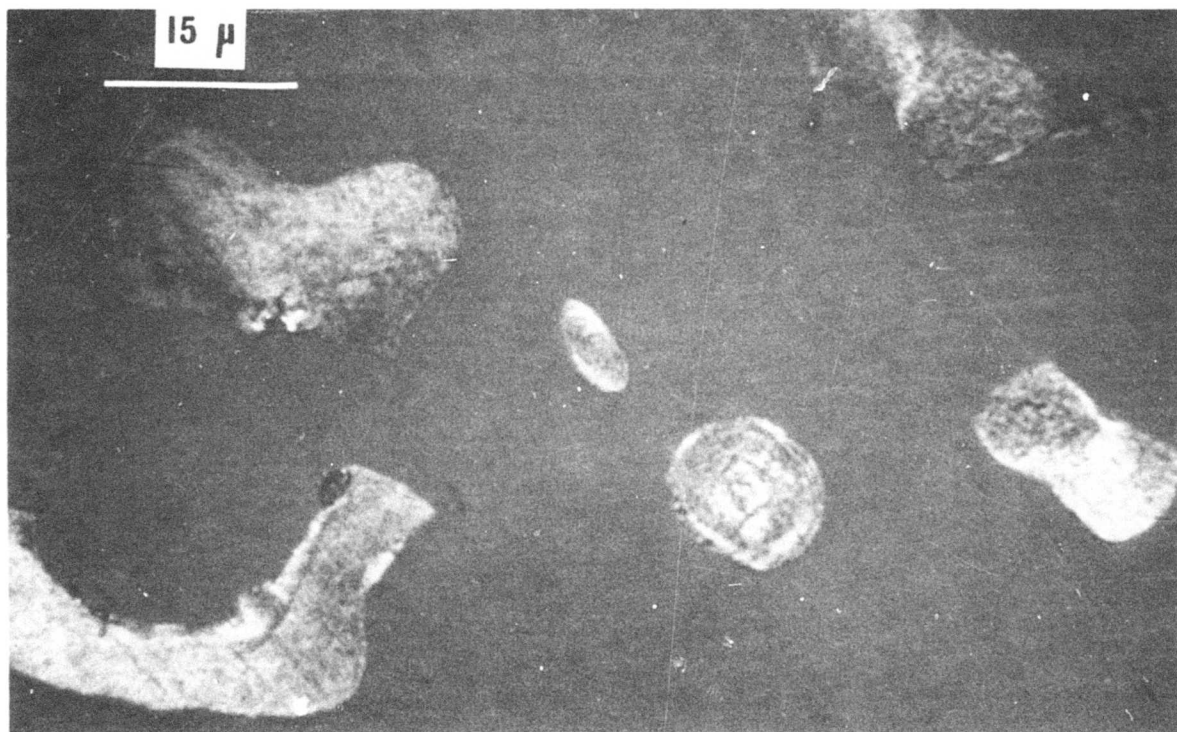
#### B. Observations and Discussions

Photomicrographs of the mounted specimens are shown in Fig. 26 to 31. The Pitch I fibers are observed to vary greatly in cross-sectional shape. In many instances, the fibers are circular

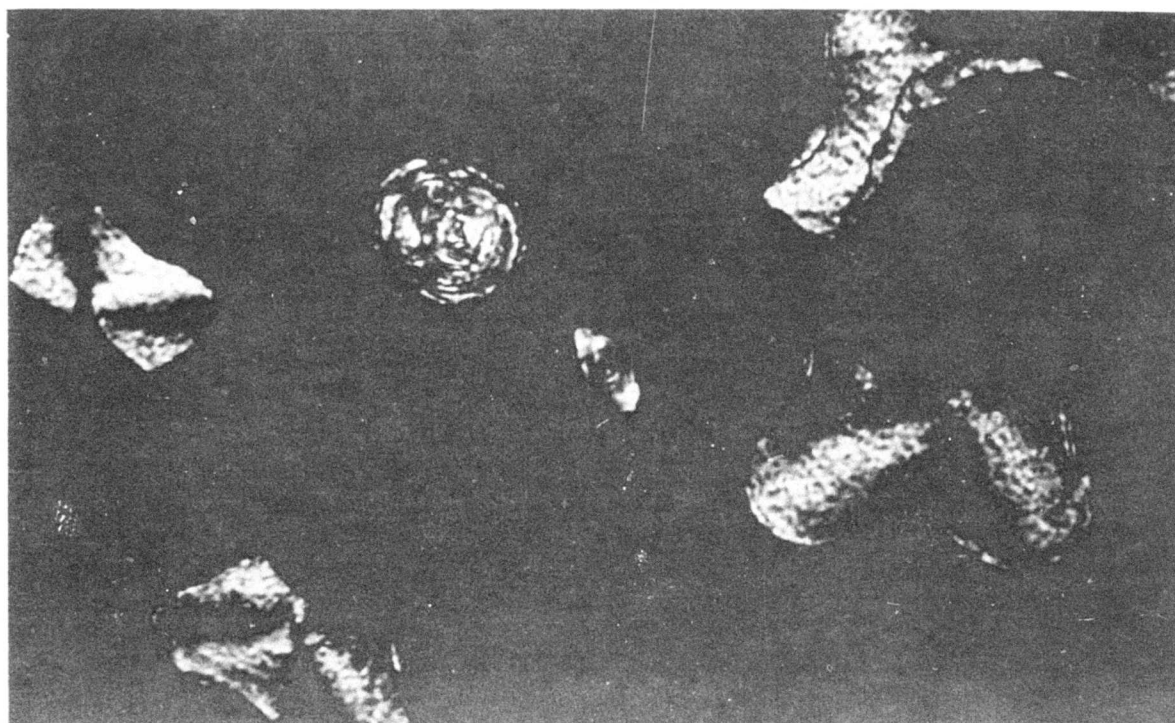
with a pie-shaped piece missing (" $\pi$ " fibers); others are round, or crescent shaped. Size as well varies significantly from 5 to 50 microns in diameter. Interestingly, there is an absence of large round fibers. The possible reasons for this are suggested by the observations made in polarized light (Figs. 26-b and 27-b). The odd-shaped (i.e. " $\pi$ ", crescent, etc.) tend to have well-developed radial structures judging from the distinct "Maltese Cross" patterns observable under polarized light. However, in most cases, the pattern is not complete. Obviously, the fibers have split at some time during their processing. This could also explain the existence of the crescent shaped fibers: as well as splitting in half, the outer shell has separated from the inner core. Further evidence for this splitting is shown in Fig. 27 where the two separate halves apparently still lie in close proximity to each other. In contrast, the round fiber in Fig. 26 shows no Maltese cross pattern at all, although there is significant optical activity. Interestingly, no "missing pieces" have been observed for the " $\pi$ " fibers, and the large opening must result from dimensional changes during processing.

Figure 28 shows Pitch I fibers at other angles of inclination as well as a longitudinal section of one fiber. The odd fiber shapes are again apparent as well as the partial Maltese cross pattern of extinction. The extinction phenomenon is again illustrated in Fig. 29. In Fig. 29-a the fiber running diagonally





(a)



(b)

Figure 26

UCC Pitch Precursor Carbon Fibers (85MSI): Cross Section

- a) Ordinary Light
- b) Polarized Light

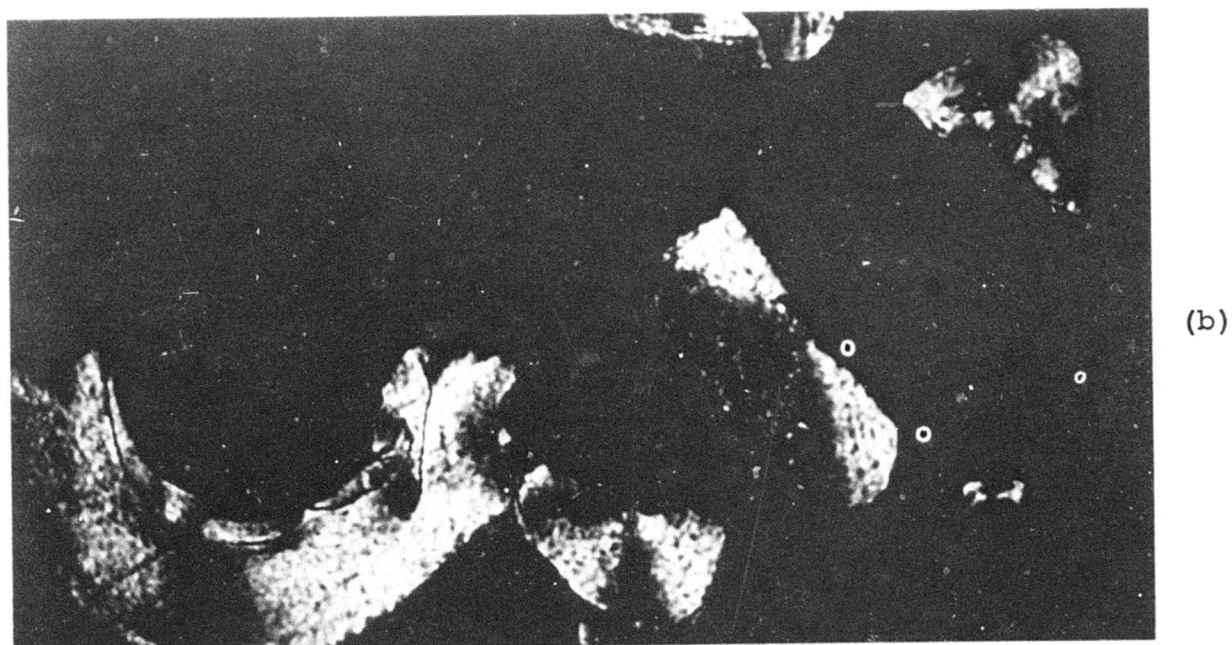
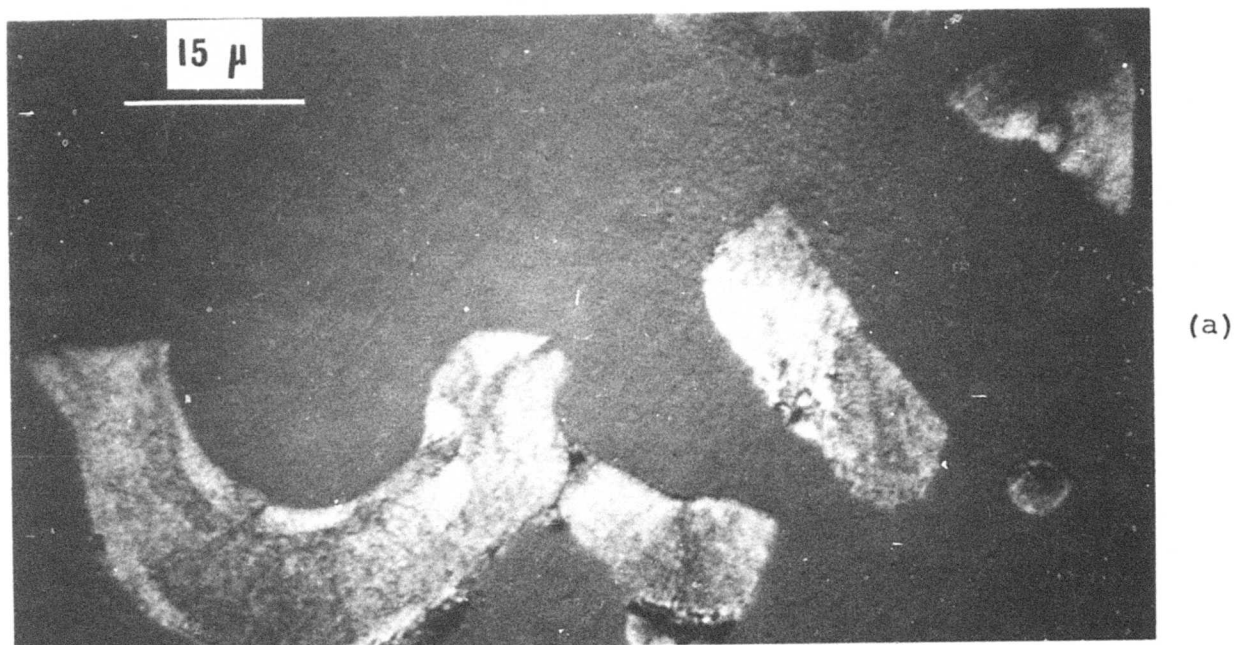


Figure 27

UCC Pitch Precur Carbon Fibers (85MSI): Cross Section

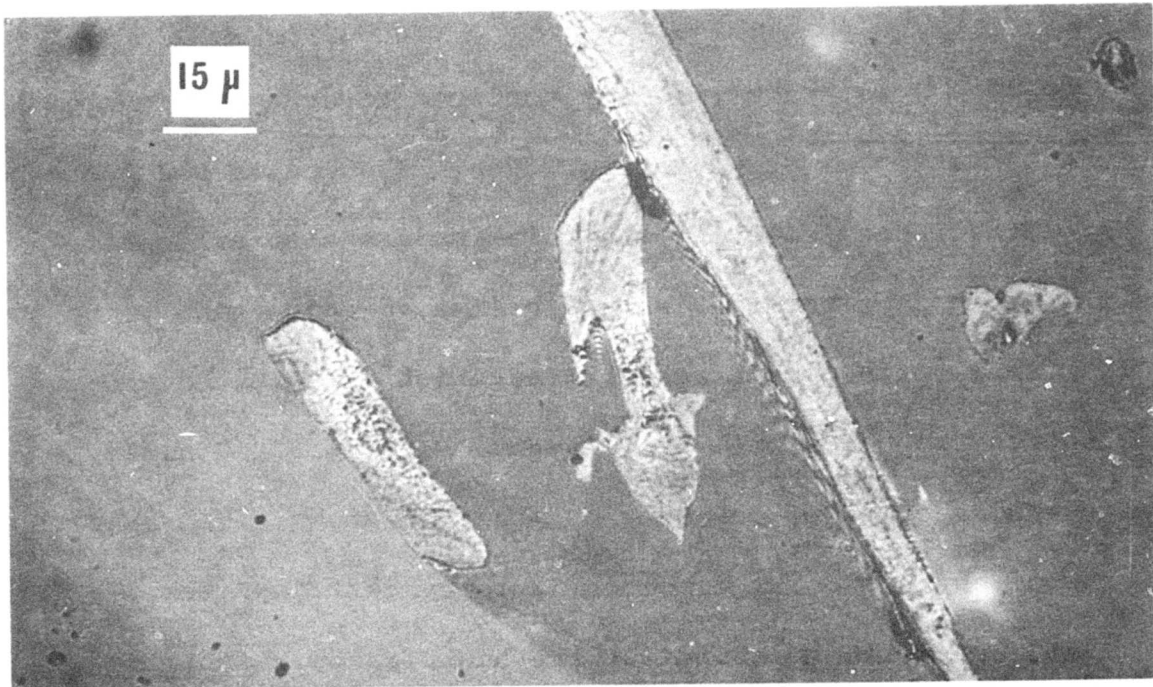
- a) Ordinary Light
- b) Polarized Light

(upper left to lower right) is extinguished after a 45° counter-clockwise rotation as shown in Fig. 29-b. Changes in the patterns of the other fibers following the rotation are also evident.

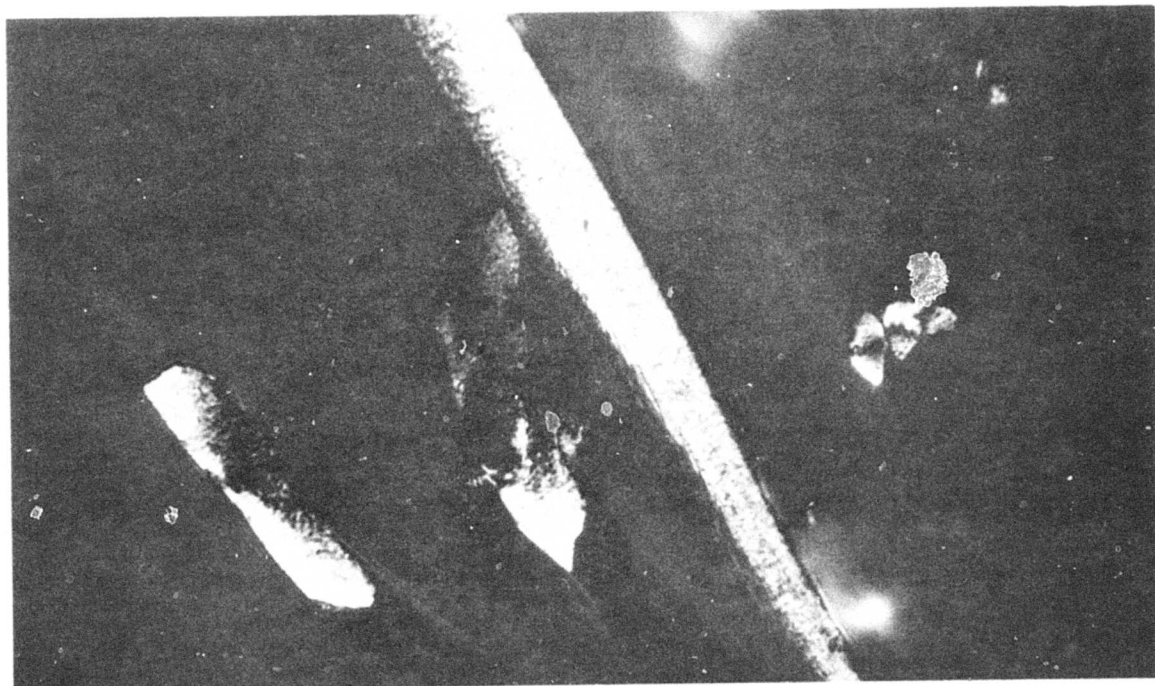
The Pitch II fibers, as shown in Figs.30 and 31, tend to be somewhat smaller in size than the others but exhibit the same basic shapes, round as well as crescent. In Fig.31, a nearly longitudinal section of one of the fibers is shown. The same patterns of extinction as in Pitch I are evident in Pitch II.

The average fiber densities were high for both fiber mats: 2.19g/cc for the high modulus fiber and 2.10g/cc for the lower modulus one. Such high densities indicate the presence of the very highly oriented fibers observed under polarized light.

These microstructures are consistent with the probable Union Carbide process as revealed by Netherlands Patent No.239490. This patent teaches that a petroleum pitch is partially converted to a mesophase (liquid crystal). This partial conversion of the pitch to mesophase would suggest that the resulting fiber mat would be composed of fibers whose structure varied depending on the presence or absence of mesophase. Certainly, there is evidence of two different structures in each of the pitch fiber mats studied. In the large fibers where the Maltese cross extinction pattern under polarized light is clear, the structure could be either spoke-like or wrap-around since both will produce such a pattern under crossed polars. A distinction between the two can be made by observing the



(a)



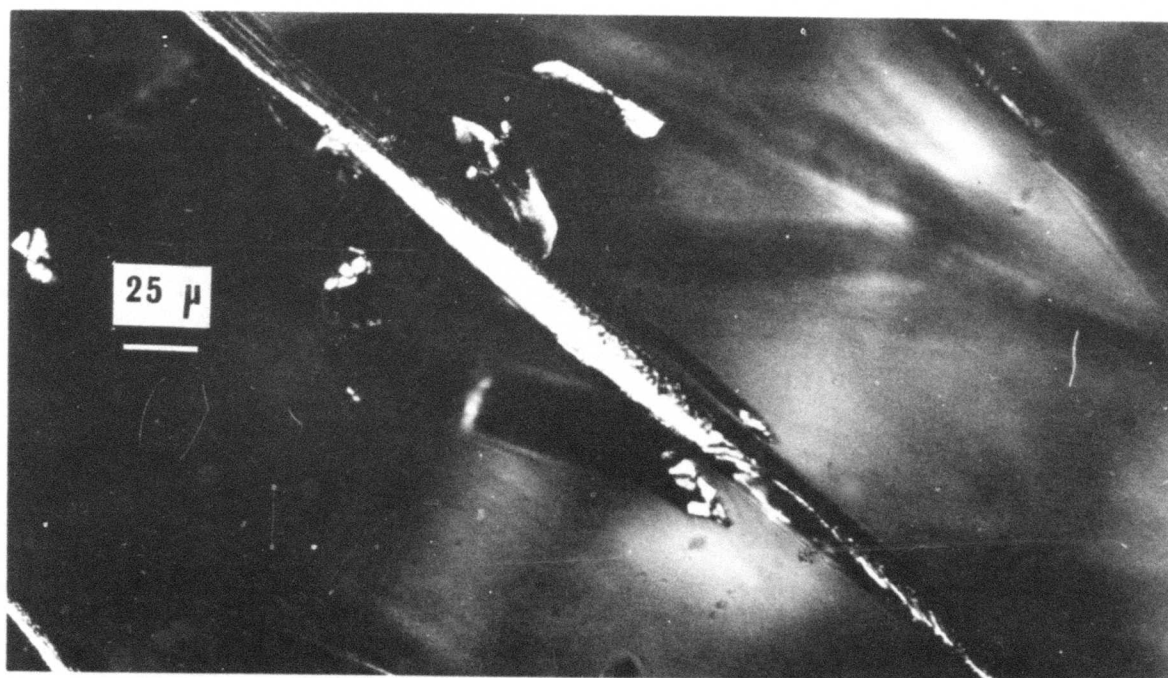
(b)

Figure 3

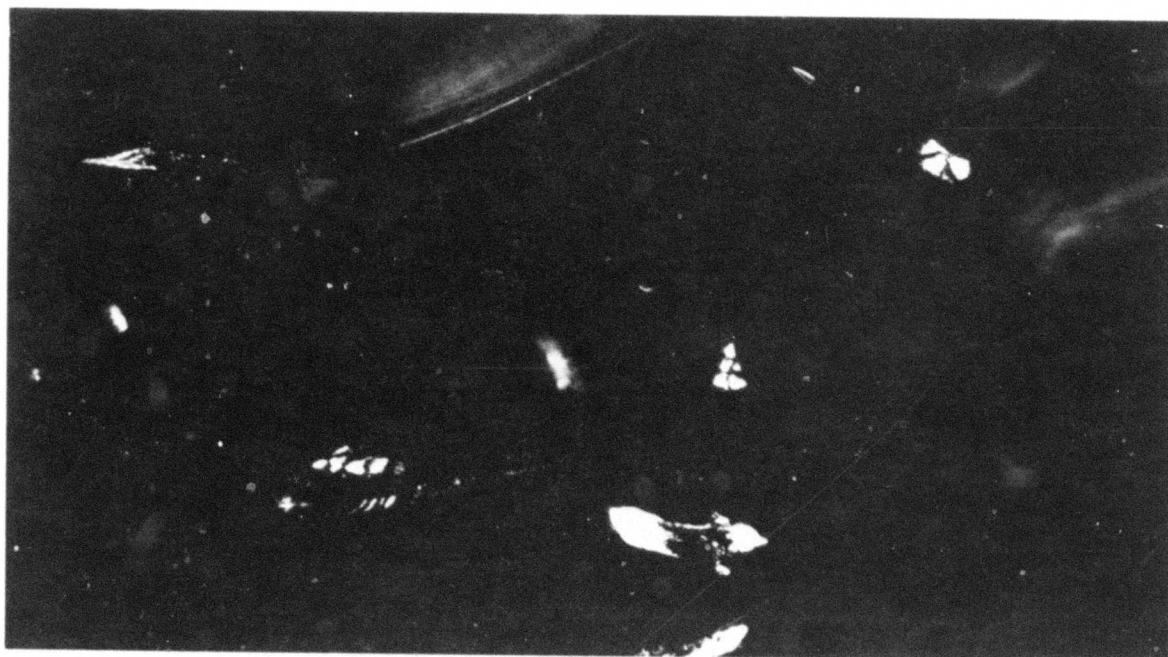
UCC Pitch Precursor Carbon Fibers (85MSI):  
Various Angles of Inclination

- a) Ordinary Light
- b) Polarized Light





(a)

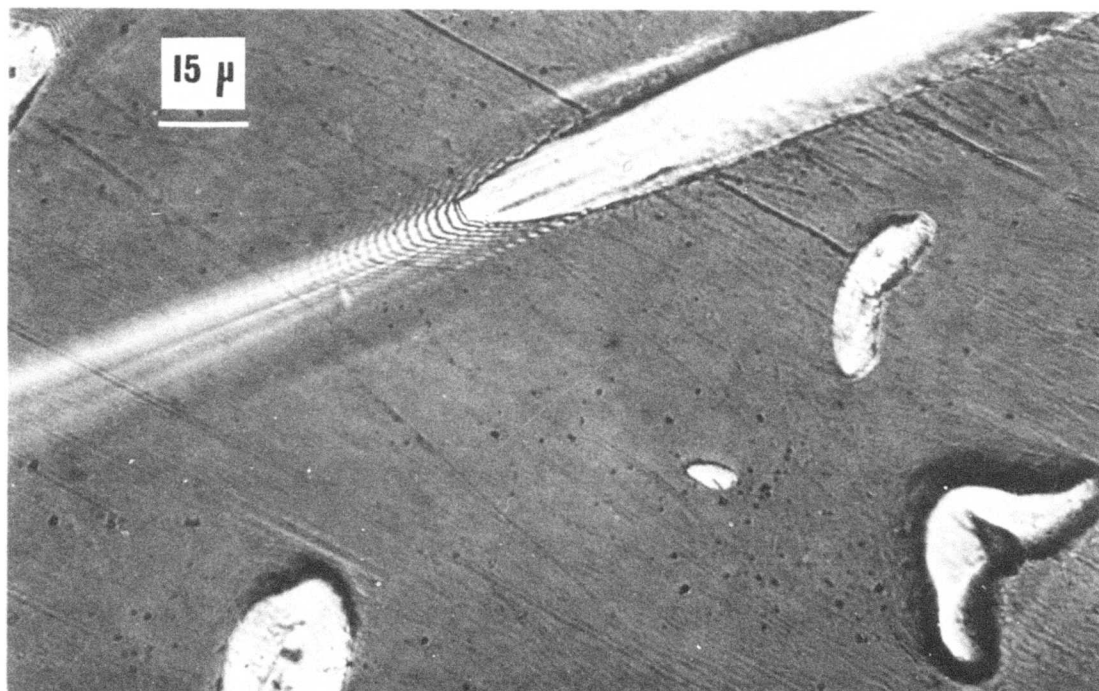


(b)

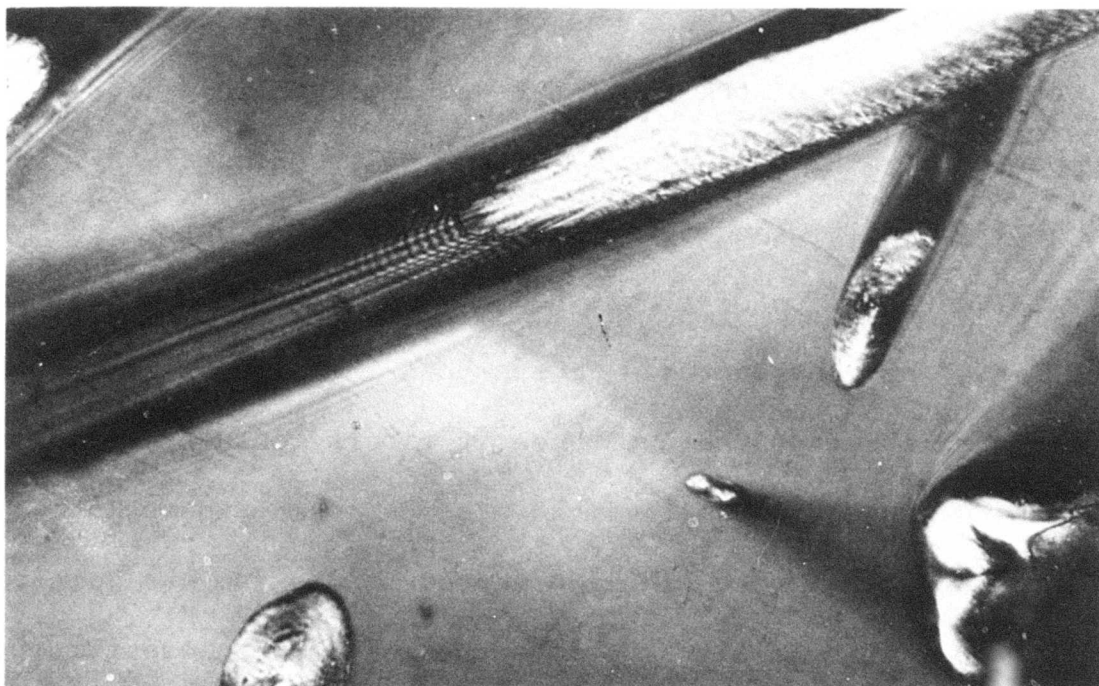
Figure 29

UCC Pitch Precursor Carbon Fibers (85MSI):  
Various Angles of Inclination

- a) Initially; Polarized Light
- b) After 45° Counterclockwise Rotation;  
Polarized Light



(a)



(b)

Figure 31

High Precursor Carbon Fibers (20-30MSI):  
Various Angles of Inclination

- a) Ordinary Light
- b) Polarized Light



(a)



(b)

**Figure 31**

**UCC Pitch Precursor Carbon Fibers (20-30MSI):  
Various Angles of Inclination**

- a) Ordinary Light
- b) Polarized Light

extinction pattern as the analyser is rotated (see Technical Report AFML-TR-72-133 Part I, Appendix II). Using this technique, the structure is observed to be spoke-like. The spoke structure might also be inferred from the "pie-with-missing-piece" shape of many of the fibers.

The structure of the smaller fibers is less clear but since the polarized light pattern is broken up, the structure is probably more irregular. As a result, it would be expected that the density of these smaller fibers would be less than the larger more regular spoke-structure fibers. This was observed to be the case in a test where a sample of the fiber mat was immersed in a liquid of approximately the same density. Some of the fibers sank, the remainder floated. When collected and observed in polarized light, the dense group of fibers had a much higher concentration of the large, spoke-structured fibers than the lighter group.

The separation of the two types of fibers would occur during the spinning process where the more viscous mesophase would be spun into the larger more highly oriented fibers and the remaining less-viscous isotropic pitch would form the smaller less structured fibers.

#### C. Conclusions

1) The high modulus pitch-based carbon fiber mat studied consists of two types of fiber which may be distinguished on the basis of optical activity under polarized light:



- a) The generally larger, denser crescent shaped fibers with a well-developed spoke-like radial structure resulting in a "Maltese Cross" polarized light extinction pattern. These fibers would form from the more viscous mesophase portion of the pitch precursor; this would account for the highly developed structure.
- b) Smaller, lighter, round fibers exhibiting considerable optical activity but no "Maltese Cross" pattern might form from the isotropic pitch hence their more irregular, radial microstructure and lower density.

2) The shapes of the fibers observed in both mats indicates that there is considerable splitting of the large mesophase fibers during the carbonizing process. This splitting could result from cool-down stresses generated within the fiber but is more likely to occur during carbonization. The shapes after splitting are consistent with the highly developed spoke-like radial structure proposed for these fibers.

3) The "composite" fiber observed occasionally would be very prone to splitting due to its dual structure, i.e. resulting from an isotropic pitch core surrounded by mesophase. This would explain its relative scarcity as well as the abundance of crescent fibers (i.e. with centers removed) and the separated cores themselves (small round fibers with less developed radial structure).

4) Splitting would also be a problem in continuous mesophase pitch fibers if the well-developed spoke-like radial structure is present, particularly for high heat-treatment temperatures where the greatest cool-down stresses would be generated. As internal shear would also be poor for highly heat-treated fibers with this

structure, the maximum heat-treatment temperature for these fibers must be restricted to below 2000°C if good composite properties are to be obtained.

5) The lower modulus pitch-based fibers studied were generally longer and had smaller cross-sections than the higher modulus ones. However, in other respects, they were similar.